



HAL
open science

Theoretical and Computational Framework for the Analysis of the Relaxation Properties of Arbitrary Spin Systems. Application to High-Resolution Relaxometry

Nicolas Bolik-coulon, Pavel Kadeřávek, Philippe Pelupessy, Jean-Nicolas Dumez, Fabien Ferrage, Samuel F Cousin

► To cite this version:

Nicolas Bolik-coulon, Pavel Kadeřávek, Philippe Pelupessy, Jean-Nicolas Dumez, Fabien Ferrage, et al.. Theoretical and Computational Framework for the Analysis of the Relaxation Properties of Arbitrary Spin Systems. Application to High-Resolution Relaxometry. *Journal of Magnetic Resonance*, 2020, 313, pp.106718. 10.1016/j.jmr.2020.106718 . hal-02986164

HAL Id: hal-02986164

<https://hal.sorbonne-universite.fr/hal-02986164>

Submitted on 2 Nov 2020

HAL is a multi-disciplinary open access archive for the deposit and dissemination of scientific research documents, whether they are published or not. The documents may come from teaching and research institutions in France or abroad, or from public or private research centers.

L'archive ouverte pluridisciplinaire **HAL**, est destinée au dépôt et à la diffusion de documents scientifiques de niveau recherche, publiés ou non, émanant des établissements d'enseignement et de recherche français ou étrangers, des laboratoires publics ou privés.

Theoretical and Computational Framework for the Analysis of the Relaxation Properties of Arbitrary Spin Systems. Application to High-Resolution Relaxometry

Nicolas Bolik-Coulon^a, Pavel Kaderávek^{a,1}, Philippe Pelupessy^a,
Jean-Nicolas Dumez^{b,*}, Fabien Ferrage^{a,*}, Samuel F. Cousin^{a,2,*}

^a*Laboratoire des Biomolécules, LBM, Département de Chimie, École Normale Supérieure, PSL University, Sorbonne Université, CNRS, 75005 Paris, France*

^b*CEISAM, CNRS, Université de Nantes, 44300 Nantes, France*

Abstract

A wide variety of nuclear magnetic resonance experiments rely on the prediction and analysis of relaxation processes. Recently, innovative approaches have been introduced where the sample travels through a broad range of magnetic fields in the course of the experiment, such as dissolution dynamic nuclear polarization or high-resolution relaxometry. Understanding the relaxation properties of nuclear spin systems over orders of magnitude of magnetic fields is essential to rationalize the results of these experiments. For example, during a high-resolution relaxometry experiment, the absence of control of nuclear spin relaxation pathways during the sample transfers and relaxation delays leads to systematic deviations of polarization decays from an ideal mono-exponential decay with the pure longitudinal relaxation rate. These deviations have to be taken into account to describe quantitatively the dynamics of the system. Here, we present computational tools to (1)

*Corresponding authors

Email addresses: Jean-Nicolas.Dumez@univ-nantes.fr (Jean-Nicolas Dumez), Fabien.Ferrage@ens.fr (Fabien Ferrage), Samuel.Cousin@ens-lyon.fr (Samuel F. Cousin)

¹Present address: Central European Institute of Technology, Masaryk University, Kamence 5, 625 00 Brno, Czech Republic

²Univ Lyon, CNRS, Université Claude Bernard Lyon 1, Ens de Lyon, Institut des Sciences Analytiques, France

calculate analytical expressions of relaxation rates for a broad variety of spin systems and (2) use these analytical expressions to correct the deviations arising in high-resolution relaxometry experiments. These tools lead to a better understanding of nuclear spin relaxation, which is required to improve the sensitivity of many pulse sequences, and to better characterize motions in macromolecules.

Keywords: Nuclear Spin Relaxation, Analytical Relaxation Computation, High-Resolution Relaxometry

1. Introduction

The development of most Nuclear Magnetic Resonance (NMR) experiments requires the understanding of relaxation properties. Improvement in the sensitivity and resolution have been obtained, ranging from the use of an optimum excitation angle with respect to the longitudinal relaxation, known as the Ernst angle [1], to the development of Transverse Relaxation Optimized Spectroscopy (TROSY) experiments [2, 3] that exploit relaxation interferences [4, 5, 6, 7]. An in depth investigation of relaxation processes is particularly critical to design and interpret several classes of experiments which are based on moving the sample through a broad range of magnetic fields. **A variety of such experiments have designed recently:** (1) The existence of Long-Lived States (LLS) [8, 9] was revealed by the combination of high-field coherent evolution and low-field relaxation; (2) In dissolution Dynamic Nuclear Polarization (dDNP) [10, 11, 12], the hyperpolarized sample is transferred back and forth between the polarizing magnetic center and the high-field spectrometer through magnetic fields that can be as low as the earth magnetic field; (3) Multi-scale dynamics can be characterized with Fast-Field Cycling (FFC) relaxometry [13] where the magnetic field is switched from *ca.* 1 T down to *ca.* 100 μ T; (4) A sample-shuttle apparatus can be used to combine relaxometry experiments with high-field NMR [14, 15, 16, 17] to gain atomic resolution description of molecular dynamics; (5) This kind of device can also be used to investigate relaxation properties of spin terms that are only relevant at low fields [18]; (6) A sample shuttle may couple two magnetic centers in a two-field NMR spectrometer [19] to record multi-dimensional experiments where spins are manipulated at two vastly different fields [19, 20, 21, 22]. Sample-shuttling experiments have been used to measure longitudinal relax-

28 ation rates over orders of magnitude of magnetic fields and characterize the
29 dynamics of membrane vesicles [23], protein backbone [24, 17] and side-
30 chains [25]. This type of experiments, called High-Resolution Relaxometry
31 (HRR), consists in the measurement of relaxation rates over a broad range of
32 magnetic field while preserving the high resolution of conventional high-field
33 magnets (*i.e.* higher than 9 T) [14, 15]. This approach relies on moving the
34 NMR sample in the stray field of a commercial magnet to measure longitudi-
35 nal relaxation rates over orders of magnitude of magnetic field. The sample is
36 transferred back in the high-field magnetic center for detection, thus ensuring
37 high sensitivity and resolution.

38 During a high-resolution relaxometry experiment, the sample is moved out-
39 side of the magnetic center where no radiofrequency pulse can be applied.
40 Thus, relaxation decays acquired using HRR suffer from two types of sys-
41 tematic errors. First, the effective density operator at the beginning of the
42 relaxation delay is usually different from the desired longitudinal operator
43 due to cross-relaxation during the sample transfers. Second, cross-relaxation
44 pathways during the relaxation delay may lead to multi-exponential polar-
45 ization decays. Therefore, the analysis of experimental HRR rates requires
46 to account for these systematic deviations in order to accurately determine
47 the motional parameters of the system under study. We introduced an it-
48 erative correction procedure called Iterative Correction for the Analysis of
49 Relaxation Under Shuttling (ICARUS) [17, 26] for the correction of HRR
50 relaxation rates. Using symbolic expressions of magnetic-field dependent
51 relaxation matrices, the HRR experiments are simulated and measured re-
52 laxometry relaxation rates are corrected so that a reliable analysis of the
53 dynamic properties of the system under study can be performed.

54 Thus, the development of tools to simulate spin relaxation for a broad variety
55 of field trajectories is of great interest, in several areas of magnetic resonance
56 [27, 28, 29]. Here, we present a toolbox that combines two programs. The
57 first one, REDKITE, provides analytical expressions of relaxation rates and
58 relaxation matrices for arbitrary spin system. The second one, ICARUS,
59 is used to retrieve accurate estimates of longitudinal relaxometry relaxation
60 rates that are further used to determine the parameters describing the dy-
61 namics of the system. ICARUS simulates the HRR experiments using ana-
62 lytical expressions obtained from REDKITE.

63 REDKITE has been written in MATHEMATICA (version 12.0) [30] to per-
64 form efficiently analytical calculations using the SPINDYNAMICA (version
65 2.15.1b10) [29] package and the so called "BRW engine" to simplify the com-

66 putation of relaxation rates [28]. This version of ICARUS has been written
 67 in PYTHON (version 3.5). This language has the advantage of being free and
 68 easy to install, allowing for relatively fast numerical evaluations, and being
 69 easy to customize by the user. ICARUS is written as a framework so that
 70 users can define the spin systems, relaxation matrices and spectral density
 71 functions relevant for their applications.

72 In this paper, we first describe succinctly our approach to calculate relaxation
 73 rates efficiently and apply this method on an isolated $^{15}\text{N}^1\text{H}$ spin system using
 74 REDKITE. We illustrate the power of these tools with a detailed presentation
 75 of the recently published analysis of carbon-13 HRR in $\{^{13}\text{C}^1\text{H}^2\text{H}_2\}$ -methyl
 76 groups in the protein Ubiquitin [25] and test the validity of key hypotheses
 77 made during the analysis. In particular, we use two-field NMR to determine
 78 the relevant interactions to describe the relaxation properties of $\{^{13}\text{C}^1\text{H}^2\text{H}_2\}$ -
 79 methyl groups, and verify the validity of the correction at 0.33 T.

80

81 **2. Theory and relaxation**

82 *2.1. Calculation of relaxation superoperators with REDKITE*

83 The full description of the Bloch-Wangsness-Redfield (BWR) relaxation
 84 theory in liquid-state NMR is beyond the scope of this article and can be
 85 found elsewhere [31, 5, 32, 33, 34]. A condensed version is presented here.

86 The evolution of the density operator $\hat{\sigma}(t)$ is described by the Liouville-von
 87 Neumann equation, **in units of \hbar** :

$$\frac{d\hat{\sigma}(t)}{dt} = -i[\hat{\mathcal{H}}(t), \hat{\sigma}(t)]. \quad (1)$$

88 The Hamiltonian $\hat{\mathcal{H}}$ of the system can be expressed as the sum of a stationary
 89 part $\hat{\mathcal{H}}_0$ and a fluctuating part $\hat{\mathcal{H}}_1(t)$:

$$\hat{\mathcal{H}}(t) = \hat{\mathcal{H}}_0 + \hat{\mathcal{H}}_1(t). \quad (2)$$

90 This equation can be transformed in the interaction frame of the stationary
 91 Hamiltonian $\hat{\mathcal{H}}_0$. An operator $\hat{\mathcal{O}}$ transformed into the interaction frame is
 92 labeled with a tilde:

$$\tilde{\hat{\mathcal{O}}}(t) = \exp(i\hat{\mathcal{H}}_0 t) \hat{\mathcal{O}}(t) \exp(-i\hat{\mathcal{H}}_0 t). \quad (3)$$

93 The frame transformation of the full Hamiltonian $\hat{\mathcal{H}}$ requires the subtraction
 94 of the Zeeman Hamiltonian $\hat{\mathcal{H}}_0$, so that the Liouville-von Neumann equation

95 now reads:

$$\frac{d\tilde{\sigma}(t)}{dt} = i[\tilde{\sigma}(t), \tilde{\mathcal{H}}_1(t)]. \quad (4)$$

96 After developing a second-order time-dependent perturbation, the Liouville-
97 von Neumann equation in the interaction frame can be written as:

$$\frac{d\tilde{\sigma}(t)}{dt} = +i[\tilde{\sigma}(0), \tilde{\mathcal{H}}_1(t)] - \int_0^t [[\tilde{\sigma}(t'), \tilde{\mathcal{H}}_1(t')], \tilde{\mathcal{H}}_1(t)] dt'. \quad (5)$$

98 In the frame of the BWR theory, the following hypotheses are made to cal-
99 culate the ensemble average of the evolution of the density operator: i) for
100 an ensemble average, denoted by the horizontal bar, $\overline{[\tilde{\sigma}(0), \tilde{\mathcal{H}}_1(t)]}$ averages
101 to zero, and ii) a time t can be found that is short enough such that the
102 evolution of the spin system is negligible on the interval $[0, t]$ but that is
103 much larger than the typical correlation times for the fluctuations of $\tilde{\mathcal{H}}_1(t)$.
104 The evolution of the density matrix $\tilde{\sigma}(t)$ over time for an ensemble average,
105 under a perturbation Hamiltonian $\tilde{\mathcal{H}}_1(t)$, can now be expressed as:

$$\overline{\frac{d\tilde{\sigma}(t)}{dt}} = - \int_0^\infty \overline{[\tilde{\mathcal{H}}_1(t), [\tilde{\mathcal{H}}_1(t+\tau), \tilde{\sigma}(t)]]} d\tau. \quad (6)$$

106 This equation can be further simplified using the irreducible tensor represen-
107 tation in order to separate the angular and spin parts of the Hamiltonian.
108 The perturbation Hamiltonian $\tilde{\mathcal{H}}_1(t)$ may include several interactions, iden-
109 tified by the label i . Each of them can be written as the sum of the product
110 of time-dependent spatial variables $V_{l,-q}(t)$ and tensor spin operators $\hat{T}_{l,q}^i$
111 of rank l and coherence order q (which is usually simply called order):

$$\hat{\mathcal{H}}_1(t) = \sum_i \zeta_i \sum_l \sum_{q=-l}^l (-1)^q V_{l,-q}^i(t) \hat{T}_{l,q}^i, \quad (7)$$

112 where ζ_i is the amplitude of the interaction i . The irreducible tensor $\hat{T}_{l,q}^i$
113 can be expressed as a linear combination of eigenoperators $\{\hat{A}_{l,q,p}^i\}$ of the
114 superoperator $[\hat{H}_0, \cdot]$, with eigenvalues $\omega_{l,q,p}^{(i)}$:

115

$$\hat{T}_{l,q}^i = \sum_p \hat{A}_{l,q,p}^i. \quad (8)$$

116 These eigenoperators can be written in the interaction frame as:

$$\tilde{A}_{l,q,p}^i(t) = \exp(i\hat{\mathcal{H}}_0 t) \hat{A}_{l,q,p}^i \exp(-i\hat{\mathcal{H}}_0 t) = e^{i\omega_{l,q,p}^{(i)} t} \hat{A}_{l,q,p}^i. \quad (9)$$

117 In the interaction frame, we now have:

$$\tilde{\mathcal{H}}_1(t) = \sum_i \zeta_i \sum_l \sum_{q=-l}^l \sum_p (-1)^q e^{i\omega_{l,q,p}^{(i)} t} V_{l,-q}^i(t) \hat{A}_{l,q,p}^i. \quad (10)$$

118 Since $\tilde{\mathcal{H}}_1$ is Hermitian, we can also write:

$$\tilde{\mathcal{H}}_1(t) = \sum_i \zeta_i \sum_l \sum_{q=-l}^l \sum_p (-1)^q e^{-i\omega_{l,q,p}^{(i)} t} V_{l,-q}^{i,*}(t) \hat{A}_{l,q,p}^{i,\dagger}, \quad (11)$$

119 where (\dagger) denotes the hermitian conjugate of the operator, and $(*)$ the com-
120 plex conjugate. Substituting Eq. 10 and 11 into Eq. 6 gives:

$$\begin{aligned} \frac{d\tilde{\sigma}(t)}{dt} = & - \sum_{i,j} \zeta_i \zeta_j \sum_{l,l'} \sum_{q=-l}^l \sum_{q'=-l'}^{l'} \sum_{p,p'} (-1)^{q+q'} e^{i(\omega_{l,q,p}^{(i)} - \omega_{l',q',p'}^{(j)}) t} \times \\ & \left[\hat{A}_{l,q,p}^i, [\hat{A}_{l',q',p'}^{j,\dagger}, \tilde{\sigma}(t)] \right] \int_0^\infty \langle V_{l,-q}^i(t) V_{l',-q'}^{j,*}(t+\tau) \rangle e^{-i\omega_{l',q',p'}^{(j)} \tau} d\tau, \end{aligned} \quad (12)$$

121 The correlation function $C_{i,j}$ between the interactions i and j is defined as:

$$\langle V_{l,-q}^i(t) V_{l',-q'}^{j,*}(t+\tau) \rangle = \frac{1}{2l+1} \delta_{q,q'} \delta_{l,l'} C_{i,j}(\tau), \quad (13)$$

122 where δ is the Kronecker delta. Oscillating terms are neglected as they
123 average to zero much faster than the evolution of the density operator (sec-
124 ular approximation) under relaxation. Thus, only secular terms for which
125 $\omega_{l,q,p}^{(i)} = \omega_{l',q',p'}^{(j)}$ contribute to Eq. 12. Only rank-2 ($l=2$) tensors are relevant
126 to describe dipole-dipole and quadrupolar interactions. For the CSA interac-
127 tion, the rank-1 tensor part (antisymmetric) is usually neglected. Note that,
128 in the presence of highly anisotropic motions, the contribution of the antisym-
129 metric CSA (rank-1 tensors) may account for up to 10% of the contribution
130 of the CSA rank-2 tensors to auto-relaxation [35, 36]. In the following, only
131 rank-2 tensors are considered.

132 The spectral density function is defined as the Fourier transform of the cor-
 133 relation function:

$$\mathcal{J}_{i,j}(\omega) = 2 \int_0^{\infty} \frac{1}{5} C_{i,j}(\tau) e^{-i\omega\tau} d\tau. \quad (14)$$

134 Inserting the spectral density function in Eq. 12 and applying the above ap-
 135 proximations leads to the following expression of the Master equation:

$$\frac{d\tilde{\sigma}(t)}{dt} = -\frac{1}{2} \sum_{i,j} \zeta_i \zeta_j \sum_{q=-2}^2 \sum_{p,p'} \delta_{\omega_{2,q,p}, \omega_{2,q,p'}^{(j)}} \mathcal{J}_{i,j}(\omega_{2,q,p}^{(i)}) \left[\hat{A}_{2,q,p}^i [\hat{A}_{2,q,p'}^{j,\dagger}, \tilde{\sigma}(t)] \right]. \quad (15)$$

136 The final step consists in transforming Eq. 6 from the interaction represen-
 137 tation back to the Schrödinger representation given in Eq. 1. For this, we
 138 invert Eq. 3:

$$\hat{\sigma}(t) = \exp(-i\hat{\mathcal{H}}_0 t) \tilde{\sigma}(t) \exp(i\hat{\mathcal{H}}_0 t), \quad (16)$$

139 with time-derivative:

$$\frac{d\hat{\sigma}(t)}{dt} = -i[\hat{\mathcal{H}}_0, \hat{\sigma}(t)] + \exp(-i\hat{\mathcal{H}}_0 t) \frac{d\tilde{\sigma}(t)}{dt} \exp(i\hat{\mathcal{H}}_0 t). \quad (17)$$

140 Inserting Eq. 15 into Eq. 17 leads to:

$$\begin{aligned} \frac{d\hat{\sigma}(t)}{dt} &= -i[\hat{\mathcal{H}}_0, \hat{\sigma}(t)] - \\ &\frac{1}{2} \sum_{i,j} \zeta_i \zeta_j \sum_{q=-2}^2 \sum_{p,p'} \delta_{\omega_{2,q,p}, \omega_{2,q,p'}^{(j)}} \mathcal{J}_{i,j}(\omega_{2,q,p}^{(i)}) \left[\hat{A}_{2,q,p}^i [\hat{A}_{2,q,p'}^{j,\dagger}, \hat{\sigma}(t)] \right]. \end{aligned} \quad (18)$$

141 We now define the relaxation super-operator $\hat{\mathcal{R}}$ as:

$$\hat{\mathcal{R}} = \frac{1}{2} \sum_{i,j} \zeta_i \zeta_j \sum_{q=-2}^2 \sum_{p,p'} \delta_{\omega_{2,q,p}, \omega_{2,q,p'}^{(j)}} \mathcal{J}_{i,j}(\omega_{2,q,p}^{(i)}) \left[\hat{A}_{2,q,p}^i [\hat{A}_{2,q,p'}^{j,\dagger}, \cdot] \right]. \quad (19)$$

142 The relaxation rate between operators \hat{A} and \hat{B} is:

$$\mathcal{R}(\hat{A}, \hat{B}) = \frac{\langle \hat{B} | \hat{\mathcal{R}} | \hat{A} \rangle}{\sqrt{\langle \hat{A} | \hat{A} \rangle \langle \hat{B} | \hat{B} \rangle}}. \quad (20)$$

143 If $\hat{A} = \hat{B}$, we speak of an auto-relaxation rate, while $\hat{A} \neq \hat{B}$ refers to a cross-
 144 relaxation rate, **if $i = j$, it is an auto-correlated relaxation rate, and if $i \neq j$**
 145 **a cross-correlation rate.** These rates can easily be calculated analytically us-
 146 ing the BRW engine [28]. It consists in calculating the double commutator
 147 for each pair of spin tensors with identical eigenfrequencies and multiply-
 148 ing them by the spectral density function evaluated at this frequency. The
 149 implementation of this algorithm in MATHEMATICA [30] is detailed for an
 150 isolated $^{15}\text{N}^1\text{H}$ spin pair (Section 3.1) and a $^{13}\text{C}^1\text{H}^2\text{H}_2$ methyl group with a
 151 vicinal deuterium (Supplementary Materials).

152 2.2. Expectation value of spin operators

153 The expectation value of a specific operator after an evolution period t is
 154 obtained from the calculation of the propagator:

$$\hat{\mathcal{P}}(t) = e^{-\hat{\mathcal{L}}t}, \quad (21)$$

155 with $\hat{\mathcal{L}}$ the Liouvillian. Eq. 21 assumes a constant Liouvillian over the in-
 156 terval t , including a constant Hamiltonian. This assumption does not hold
 157 when pulses are applied, or in field-varying experiments, such as in dDNP or
 158 relaxometry. In dDNP, the sample is polarized using a microwave source at
 159 a specific field outside the NMR spectrometer, dissolved and pushed into the
 160 spectrometer, so that the sample experiences successively: the static field of
 161 the polarizer, the fields of the trajectory between the polarizer and the spec-
 162 trometer, and the static field of the NMR spectrometer [10]. In a relaxometry
 163 experiment, the fields during the polarization, relaxation and detection pe-
 164 riods are potentially all different [13, 15]. In these cases, the evolution time
 165 t is decomposed in periods that are small enough so that the field can be
 166 considered constant, and the propagator equals:

$$\hat{\mathcal{P}}(t) = d\hat{\mathcal{P}}_n(\delta t_n, B_n) \times \dots \times d\hat{\mathcal{P}}_1(\delta t_1, B_1), \quad (22)$$

167 where $d\hat{\mathcal{P}}_i$ is the propagator during the interval δt_i for which the magnetic
 168 field equals B_i .

169 When pulses are applied, which is typically the case in standard pulse se-
 170 quences for the measurement of relaxation rates [37], cross-relaxation path-
 171 ways may no longer be active and Eq. 22 can be simplified using averaged
 172 Liouvillian theory [38, 39]. For example, for the measurement of longitu-
 173 dinal relaxation rates of nitrogen-15 in a $^{15}\text{N}^1\text{H}$ spin pair, proton π -pulses

174 are applied during the relaxation delay. In the absence of such pulses, the
 175 Liouvillian reads:

$$\hat{\mathcal{L}} = \begin{pmatrix} R_1^N & \sigma_{\text{NH}} & \delta_N \\ \sigma_{\text{NH}} & R_1^H & \delta_H \\ \delta_N & \delta_H & R_{\text{NH}} \end{pmatrix}, \quad (23)$$

176 where the relaxation matrix has been written in the basis formed by the
 177 spin operators $\{\hat{N}_z, \hat{H}_z, 2\hat{N}_z\hat{H}_z\}$ and R_1^N (respectively R_1^H) refers to nitrogen-
 178 15 (respectively proton) longitudinal relaxation rate, R_{NH} to the two-spin
 179 order relaxation rate, σ_{NH} to the dipole-dipole (DD) cross-relaxation rate
 180 between the nitrogen-15 and proton, and δ_N (respectively δ_H) to the CSA-DD
 181 cross-correlated cross-relaxation rate involving the nitrogen-15 (respectively
 182 proton) CSA. After applying a proton π -pulse, the Liouvillian is transformed
 183 according to:

$$\hat{\mathcal{L}}' = \hat{P}_\pi \hat{\mathcal{L}} \hat{P}_\pi, \quad (24)$$

184 where \hat{P}_π is the propagator for an ideal proton π -pulse:

$$\hat{P}_\pi = \begin{pmatrix} 1 & 0 & 0 \\ 0 & -1 & 0 \\ 0 & 0 & -1 \end{pmatrix}. \quad (25)$$

185 When the evolution delay before and after the pulse are equal, the proton
 186 inversion pulse leads to the following average Liouvillian over the whole re-
 187 laxation period:

$$\hat{\mathcal{L}}_{av} = \begin{pmatrix} R_1^N & 0 & 0 \\ 0 & R_1^H & \delta_H \\ 0 & \delta_H & R_{\text{NH}} \end{pmatrix}. \quad (26)$$

188 Over this time period, the spin operator \hat{N}_z is an eigenvector of the relaxation
 189 matrix, and the time-evolution of its expectation value is given by:

$$\langle \hat{N}_z \rangle(t) = e^{-R_1^N t}, \quad (27)$$

190 which is the usual mono-exponential decay used for the analysis of relaxation
 191 rates measurements (note that the evolution towards an effective saturated
 192 state is obtained from the averaging of consecutive scans [22, 40]). By con-
 193 trast, an accurate analysis of relaxation properties in the absence of radio-
 194 frequency pulses, or in field-varying experiments, requires the full relaxation
 195 matrix.

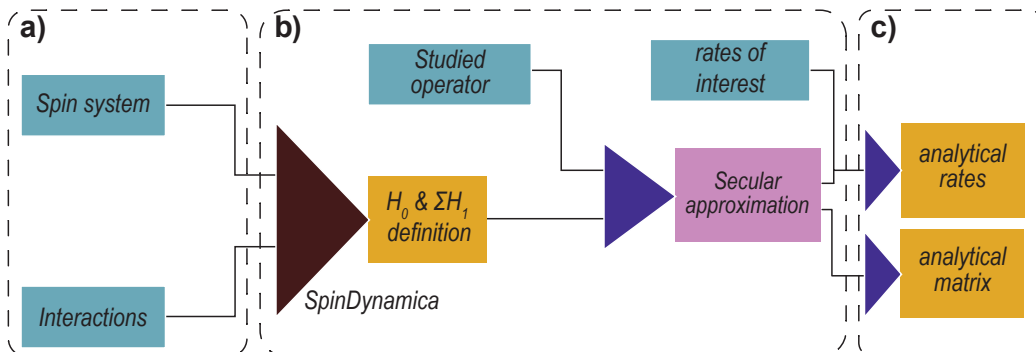


Figure 1: Schematic representation of the REDKITE calculation, describing input information and the output of the Mathematica notebook. **a)** Initial inputs from the user are the spin system (isotopes and geometry) and CSA and quadrupolar interactions. **b)** After definition of the operator basis, Hamiltonian operators are defined. After indicating the operator of the basis studied during the experiment, a reduction of the size of the basis is performed. Rates of interest are defined as well. **c)** Calculations produce analytical expressions for the relaxation rates and the relaxation matrix. Blue rectangles: user inputs. Yellow rectangles: calculated outputs. Pink rectangle and purple triangles: tasks performed by REDKITE.

196 3. Implementation and usage

197 3.1. REDKITE in Mathematica

198 The computation of the relaxation rates is highly efficient with the for-
 199 malism of the BRW engine [28] which does not require an explicit expression
 200 of the Wigner matrices defining the correlation function (Eq. 13). Relax-
 201 ation rates are first expressed as a function of the spectral density function
 202 $\mathcal{J}(\omega, \theta_i, \theta_j)$ where θ_k is the orientation of the interaction k in the system frame
 203 (SF) of the chemical moiety. This frame corresponds to an arbitrary frame in
 204 which the orientation of the interactions are calculated. The different steps
 205 of REDKITE are presented in the flowchart shown in Fig. 1. We will illustrate
 206 the use of REDKITE on an isolated pair of spin-1/2 nuclei: a ^{15}N - ^1H pair.
 207 We have used REDKITE to analyse HRR data recorded on $^{13}\text{C}^1\text{H}^2\text{H}_2$ specif-
 208 ically labelled isoleucine- δ 1 methyl groups of the protein Ubiquitin [25], and
 209 to study the relaxation properties of $^{13}\text{C}^1\text{H}_3$ methyl groups during a HZQC
 210 experiments [41].

211 *3.1.1. Definition of the spin system*

212 The first step is to define the spin system by specifying for each nuclear
213 spin the nucleus type with its isotopic number, and a unique label for each
214 spin which is used for identification. We present as an illustration the example
215 of a simple spin system composed of an isolated ^{15}N - ^1H pair. The spin system
216 is therefore defined as:

217
$$\text{Nuclei} = \{\{ "15\text{N}", "NA" \}, \{ "1\text{H}", "HA" \} \};$$

218 where "NA" and "HA" refer to the Nitrogen-15 and Proton respectively,
219 before running the SPINDYNAMICA [29] SetSpinSystem command:

220
$$\text{SetSpinSystem}[\text{Table}\{\{\text{Nuclei}[[i, 2]], \text{NuclearSpinQuantumNumber}[\text{Nuclei}[[i,$$

221
$$1]]\}], \{i, 1, \text{Length}[\text{Nuclei}]\}];$$

The NuclearSpinQuantumNumber command is implemented in SPINDYNAMICA [29] and defines the quantum spin number of the considered nucleus.

The geometry of the spin system is defined next. We define an array of size $n \times 3$ (where n is the number of nuclei in the spin system, in our case 2) containing the position of each atom in a Cartesian axis system. In our example, we set the nitrogen nucleus at the origin of the axis system and the proton 1.02 \AA away from the nitrogen in the z -direction:

$$\text{Coordinates} = \{\{0, 0, 0\}, \{0, 0, 1.02 \times 10^{-10}\}\};$$

To complete the definition of the spin system, the Chemical Shift Anisotropy (CSA) and quadrupolar properties have to be defined. The nuclei for which the CSA will be considered must be defined as such. In our example, we will only consider the nitrogen CSA:

$$\text{CSAConsidered} = \{1, 0\};$$

It is possible to give a numerical value to the CSA or keep its value as an analytical parameter. We will consider this latter case here:

$$\delta_{csa}[1] = \Delta\sigma_N;$$

222 Note that defining $\delta_{csa}[2]$ is not necessary since the proton CSA is neglected.
223 Similarly, the strength of the quadrupolar interaction does not need to be
224 defined (see in the Supplementary Materials for an example that includes

225 quadrupolar interactions).
226 The orientations of the CSA tensor have to be given (either numerically or
227 analytically). For the sake of simplicity, we choose an alignment along the
228 N-H axis:

$$229 \quad \text{vectorNum}_1^{\text{CSA}} = \{0, 0, 1\};$$

230 The index 1 refers to the first spin in the spin system (*i.e.* the nitrogen-
231 15). There is also a possibility to consider asymmetric CSA tensors. In this
232 case, the asymmetric CSA tensor is decomposed in two axially symmetric
233 components. The longitudinal and orthogonal component of the CSA have to
234 be defined using the variables names $\sigma_{\text{long}}[i]$ and $\sigma_{\text{perp}}[i]$ for the longitudinal
235 and orthogonal values of the CSA tensors of isotope i , and $\text{vectorNum}_i^{\text{CSA}}$
236 and $\text{vectorNum}_i^{\text{CSA}}$ for the associated orientations. Table S2 contains the
237 definitions of the different variables of REDKITE.

238 3.1.2. Definition of spin tensors and Hamiltonian

239 Three different types of interactions are considered in REDKITE: the
240 dipolar couplings, the CSA (in the case where at least one spin has a CSA)
241 and the quadrupolar couplings (in the case where spins with $m_s > 1/2$ are
242 present in the spin system). Analytical forms of these Hamiltonian operators
243 are calculated automatically. Other Hamiltonian operators can be defined
244 and added if other interactions or effects are considered.

245 Calculation of Hamiltonian operators requires the definition of spin-tensor
246 operators. SPINDYNAMICA already contains their definition, but each tensor
247 of coherence order- q is given as a linear combination of eigentensors [29].
248 **Consequently, SPINDYNAMICA tensors can be linear combinations of eigen-**
249 **vectors with different eigenfrequencies, which is an inappropriate basis to**
250 **perform the secular approximation (based on the equality of eigenfrequen-**
251 **cies of two eigenvectors).** The secular approximation is better performed
252 with complete separation of the tensor operators. The definition of each ten-
253 sor has already been reported for each considered interactions (dipole-dipole,
254 CSA and quadrupolar) [42] and their definition in MATHEMATICA can be
255 found in Tables S3-S5. In the case of non-equivalent homonuclear spin sys-
256 tems, performing the secular approximation is more complex, especially at
257 low fields, where the oscillation frequency in Eq. 12 can be comparable to
258 the relaxation rates. Numerical tools, such as SPINACH [28], are available to
259 study such systems. The Hamiltonian, as written in REDKITE, can be found
260 in the Supplementary Materials.

261 In the definition of the Hamiltonian, we introduce the function \mathbf{M} , similarly
 262 to the BRW engine [28], which depends on the operator coherence order m
 263 being considered, its associated eigenfrequency, a time t at which the Hamil-
 264 tonian is calculated, and the orientation of the interaction. The function \mathbf{M}
 265 is useful when calculating the double commutators to obtain relaxation rates
 266 (as detailed in Section 2.1). Products of the function \mathbf{M} appear, which are
 267 simplified according to:

$$268 \quad \mathbf{M}[l_ , f1_ , 0, i_] \text{Conjugate}[\mathbf{M}[k_ , f2_ , t_ , j_]] := \text{KroneckerDelta}[l, k] \\ 269 \quad \text{KroneckerDelta}[f1, f2] G[t, f1, i, j];$$

270 where $\text{KroneckerDelta}[x, y] = 1$ if $x = y$ and 0 otherwise, l and k are associ-
 271 ated to tensor coherence order, $f1$ and $f2$ to the tensor eigenfrequencies, t the
 272 time at which the Hamiltonian is calculated, and i and j are the orientation
 273 of the interactions in the molecular frame. $G[t, f1, i, j]$ is the correlation
 274 function evaluated at time t and is further replaced by the spectral den-
 275 sity function evaluated at frequency $f1$. For auto-correlation, $i = j$, while
 276 cross-correlation is obtained when $i \neq j$.

277 3.1.3. Operator of interest

278 We define the operator of interest as the initial state where the polariza-
 279 tion has been stored. In HRR, it is the longitudinal Zeeman term. In our
 280 case, we are interested in the nitrogen-15 longitudinal relaxation rates, which
 281 is defined by:

$$282 \quad \text{OperatorOfInterest} = \text{opI}["\text{NA}", "z"];$$

283 where `opI` is a SPINDYNAMICA [29] command to define operators, here the
 284 N_z operator.

285 3.1.4. Analytical and numerical spin state restriction

The number of terms in the basis is equal to 4^n for n spin-1/2 nuclear spins. Hence, in this two-spin system there are 16 terms, which is still a workable number. For more complex spin systems, reducing the size of the basis is essential. We only keep the terms contributing to the relaxation of the operator of interest following the scheme of Fig. 2. First, only terms with the same coherence order as the operator of interest are selected (indicated in blue in Fig. 2a). Then, the secular approximation removes all non-secular terms in the interaction frame (Fig. 2b). Cross-relaxation rates with the operator of

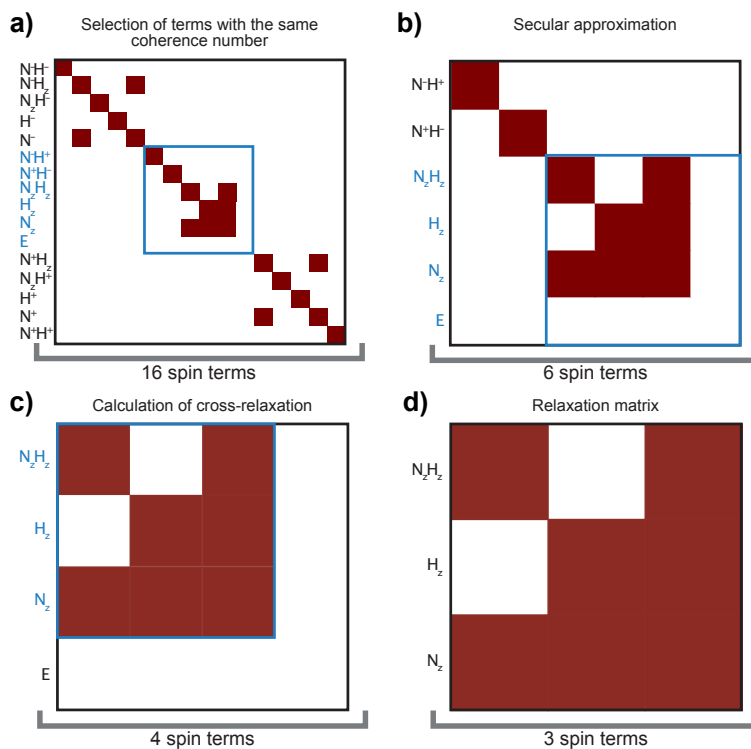


Figure 2: Reduction of the matrix size for our case example of a $^{15}\text{N}-^1\text{H}$ spin system. **a)** A $^{15}\text{N}-^1\text{H}$ isolated spin pair has 16 operators in its basis. **b)** The first step of the matrix reduction size consists in keeping only terms that have the same coherence order as the spin-term of interest, leading to 6 terms in the basis. **c)** The secular approximation allows another level of size reduction: only terms that are secular with the Zeeman Hamiltonian are kept in the basis. Two terms are removed at this stage. **d)** In the absence of cross-relaxation with the spin term of interest N_z , the identity operator is removed from the basis and the final basis contains 3 operators. In this graphical representation of the relaxation matrices, a red square indicates a non-zero value for the corresponding relaxation rate. The blue rectangles contain the selected part of the relaxation matrix after each steps of the size reduction. Normalization factors for the spin operators have been omitted for clarity.

interest in this reduced basis are calculated (Fig. 2c) and the operators with no cross-relaxation with the operator of interest are discarded from the basis (here this last step only removes the identity operator E , Fig. 2d). This step is basis-dependent and some indirect cross-relaxation pathways affecting the operator of interest may be suppressed. An additional step can be applied for large spin systems to sort and select only major cross-relaxation pathways. In our example of an isolated ^{15}N - ^1H spin pair with a CSA on the nitrogen-15, only 3 terms remain in the basis:

$$\text{ReducedBasis} = \{\text{NA}_z, \text{HA}_z, 2\text{NA}_z\text{HA}_z\};$$

286 3.1.5. Calculations

Once the basis has been defined, the relaxation matrix can be calculated:

$$\text{RM} = \begin{pmatrix} R_1^{\text{N}} & \sigma_{\text{NH}} & \delta_{\text{N}} \\ \sigma_{\text{NH}} & R_1^{\text{H}} & 0 \\ \delta_{\text{N}} & 0 & R_{\text{NH}} \end{pmatrix},$$

287 where R_1^{N} and R_1^{H} refer to the nitrogen-15 and proton longitudinal relaxation
 288 rates respectively, R_{NH} to the auto-relaxation rate of the two-spin order, σ_{NH}
 289 to the dipole-dipole cross-relaxation rate between nitrogen-15 and proton
 290 and δ_{N} to the CSA-(dipole-dipole) cross-relaxation rate due to the cross-
 291 correlation of the nitrogen-15 CSA and the dipole-dipole coupling:

$$\begin{aligned} R_1^{\text{N}} &= \frac{d_{\text{NH}}^2}{2} (\mathcal{J}(\omega_{\text{N}} - \omega_{\text{H}}) + 6\mathcal{J}(\omega_{\text{N}} + \omega_{\text{H}}) + 3\mathcal{J}(\omega_{\text{N}})) + \frac{2\sigma_{\text{N}}^2}{3} \Delta\sigma_{\text{N}}^2 \omega_{\text{N}}^2 \mathcal{J}(\omega_{\text{N}}), \\ R_1^{\text{H}} &= \frac{d_{\text{NH}}^2}{2} (\mathcal{J}(\omega_{\text{N}} - \omega_{\text{H}}) + 6\mathcal{J}(\omega_{\text{N}} + \omega_{\text{H}}) + 3\mathcal{J}(\omega_{\text{H}})), \\ R_{\text{NH}} &= \frac{3d_{\text{NH}}^2}{2} (\mathcal{J}(\omega_{\text{N}}) + \mathcal{J}(\omega_{\text{H}})) + \frac{2}{3} \Delta\sigma_{\text{N}}^2 \omega_{\text{N}}^2 \mathcal{J}(\omega_{\text{N}}), \\ \sigma_{\text{NH}} &= \frac{d_{\text{NH}}^2}{2} (-\mathcal{J}(\omega_{\text{N}} - \omega_{\text{H}}) + 6\mathcal{J}(\omega_{\text{N}} + \omega_{\text{H}})), \\ \delta_{\text{N}} &= 2\Delta\sigma_{\text{N}} \omega_{\text{N}} d_{\text{NH}} \mathcal{J}(\omega_{\text{N}}), \end{aligned}$$

292 with $d_{\text{NH}} = -\frac{\mu_0}{4\pi} \frac{\hbar\gamma_{\text{H}}\gamma_{\text{N}}}{r_{\text{NH}}^3}$ the dipolar coefficient between the proton and the
 293 nitrogen-15, r_{NH} the distance separating the two nuclei, γ_X the gyromagnetic
 294 ratio of nucleus X , \hbar the Plank constant divided by 2π , μ_0 the permeability
 295 of free space, and $\Delta\sigma_{\text{N}} = \sigma_{zz} - \frac{\sigma_{xx} + \sigma_{yy}}{2}$ the CSA of the nitrogen-15 with σ_{kk} the
 296 k^{th} diagonal element of the chemical shift tensor. \mathcal{J} is the spectral density

297 function and is expressed as a function of the proton (ω_H) and nitrogen-15
 298 (ω_N) Larmor frequencies.
 299 All types of relaxation rates in this spin system can be calculated. In such a
 300 spin system, it is relatively easy to record longitudinal and transverse relax-
 301 ation rates for the nitrogen-15 nucleus, as well as the cross-relaxation rate
 302 with the proton. These rates are calculated by:

```
303 RatesOfInterest = {
304   {Rate[opI["NA", "z"], opI["NA", "z"]], "R1N"},
305   {Rate[opI["NA", "+"], opI["NA", "+" ]], "R2N"},
306   {Rate[opI["NA", "z"], opI["HA", "z"]], "Sigma"}};
```

where Rate is the implemented command to calculate relaxation rates as described in the previous section. This leads to the expression of transverse relaxation rate for nitrogen-15:

$$R_2^N = \frac{d_{\text{NH}}^2}{4} (\mathcal{J}(\omega_N - \omega_H) + 6\mathcal{J}(\omega_N + \omega_H) + 3\mathcal{J}(\omega_N) + 6\mathcal{J}(\omega_H) + 4\mathcal{J}(0)) \\ + \frac{\Delta\sigma_N^2 \omega_N^2}{9} (3\mathcal{J}(\omega_N) + 4\mathcal{J}(0)).$$

307 3.1.6. Model selection and formatting

The user has to provide at least one definition of spectral density function in order to have a model for the dynamics of the system. In our case, we can use a model-free approach [43] with a correlation time for global tumbling τ_c , one order parameter S^2 and an effective correlation time for internal motions τ_{int} :

$$\mathcal{J}(\omega) = \frac{1}{5} \left(\frac{S^2 \tau_c}{1 + (\omega \tau_c)^2} + \frac{(1 - S^2) \tau'_{int}}{1 + (\omega \tau'_{int})^2} \right),$$

where $\tau'^{-1}_{int} = \tau_c^{-1} + \tau_{int}^{-1}$. This function is implemented in REDKITE as:

$$\text{JNH}[\omega_ , i_ , j_] := \text{Module}[\{\text{spec}, \tau 1\}, \\ \tau 1 = \tau_c \tau_i / (\tau_c + \tau_i); \\ \text{spec} = \frac{1}{5} \left(S^2 \frac{\tau_c}{1 + (\omega \tau_c)^2} + \right. \\ \left. (1 - S^2) \frac{\tau 1}{1 + (\omega \tau 1)^2} \right)]$$

308 At this point, the relaxation rates seen above can be expressed as a function
 309 of the parameters of dynamics in the system (order parameter and correlation

310 times). Numerical calculations can be performed if values for the parameters
311 of the spectral density function are provided.

312 3.1.7. *Preparing for ICARUS*

In order to use the results obtained in REDKITE for the analysis of HRR, symbolic expressions have to be exported. Exporting to ICARUS requires that all variables have Latin-only characters as the interpretation of non-Latin characters is not implemented in ICARUS. During the export process, the spectral density function is provided by the user as:

$$\text{JofInterest} = \text{JNH};$$

313 The user can export the first derivatives of the relaxation rates with re-
314 spect to all the variables (magnetic field excluded as it is not useful in the
315 following analysis). All the expressions of the relaxation matrix and the re-
316 laxation rates (and first derivatives if required) are saved in separate files
317 named respectively `RelaxationMatrix.txt` for the entire relaxation matrix,
318 `Rate.txt` for the relaxation rates defined in the `RatesOfInterest` array, and
319 `Ratederiv_Variable.txt` where *Rate* refers to the considered relaxation rate
320 and *Variable* to the variable name by which the rate is derivated. The first
321 derivatives of the relaxation rates can be used in minimization procedures.
322 An additional file named `PositionOfInterest.txt` is also created and contains
323 the position of the operator of interest in the relaxation matrix (\hat{N}_z in our
324 case example).

325 3.2. *ICARUS implementation*

326 In this paper, we show as an example how REDKITE can be used for
327 the analysis of HRR experiments. Other applications of REDKITE have
328 been published elsewhere [44, 41], and can be envisioned, as relaxation rates
329 can be obtained for any spin system. We detail here the analysis of HRR
330 relaxation rates.

331 3.2.1. *Accurate estimation of relaxation rates from high-resolution relaxom-* 332 *etry measurements*

333 High-resolution relaxometry can be used to obtain a precise description
334 of the dynamics of spin systems over orders of magnitude of timescales
335 [17, 25, 26]. The analysis is based on the measurement of longitudinal relax-
336 ation rates over a broad range of magnetic fields (typically from a few tenths

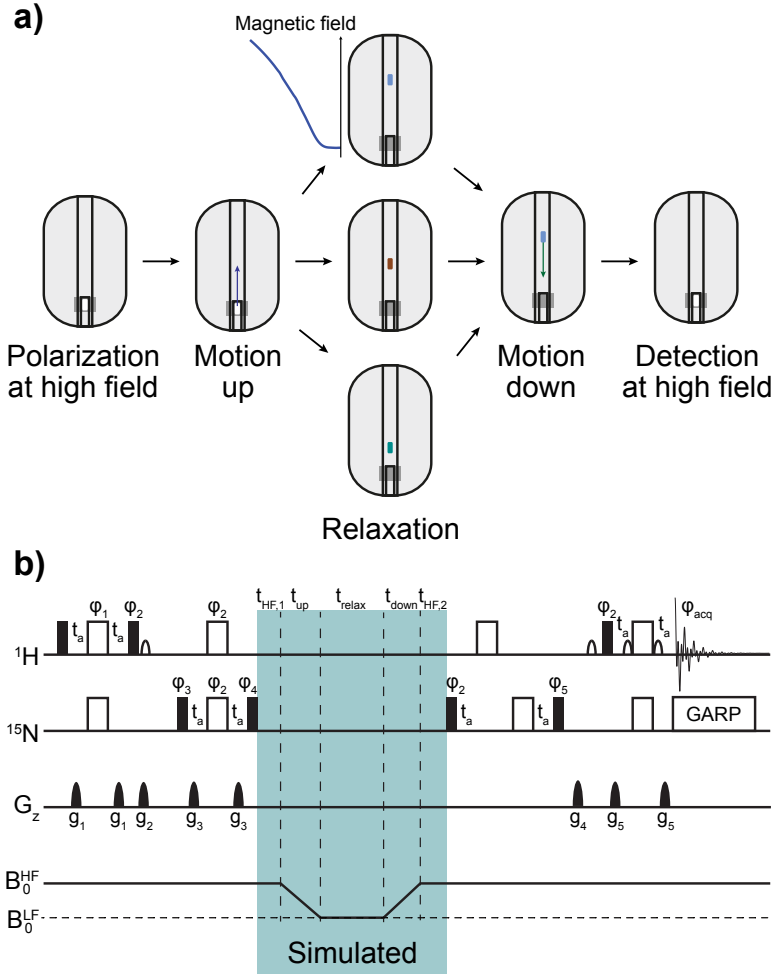


Figure 3: Description of an HRR scheme. **a)** The position of the sample is changed during the course of the experiment. It is first polarized at high field, and transferred to a chosen position in the stray field of the superconducting magnet, characterized by a lower magnetic field, for relaxation. The sample is then moved back to the high-field position for detection. Pannel adapted from [25]. **b)** A typical pulse sequence used to record HRR experiment. During the analysis of HRR rates, the highlighted part of the pulse sequence (blue) is simulated. Black narrow (respectively wide empty) rectangles represent $\pi/2$ -pulses (respectively π -pulses). Pulses are applied along the x-axis if not otherwise stated (by the φ_i). The amplitude of pulse field gradients are labeled g_i . Additional experimental details can be found in [26].

337 of Tesla up to about 20 T). A reliable description of the motions requires
 338 accurate estimates of the relaxation rates.
 339 During each high-resolution relaxometry experiment, the sample is trans-
 340 ferred outside of the magnetic center to a defined position z_{relax} in the stray
 341 field above the magnet (Fig. 3). During the two transfers (from high to low
 342 field, and back) and the relaxation delay, all relaxation pathways are active.
 343 In contrast to the example presented in Section 2.2, measured polarization
 344 decays can be affected by cross-relaxation and therefore cannot be used as
 345 is to determine longitudinal relaxation rates accurately (this is true for any
 346 relaxation experiment where pulses can not be applied during the relaxation
 347 period). Doing so would lead to systematic deviations in the parameters used
 348 to describe the dynamics of the system. Simulating the experiment including
 349 the time when the sample is outside the superconducting coil allows one to
 350 take into account cross-relaxation pathways and to estimate accurate relax-
 351 ation rates. The complete relaxation period in a high-resolution relaxometry
 352 experiment includes three delays at constant fields and two transfers through
 353 a strong gradient of magnetic field.
 354 The simulation of the experiment is performed by calculating the propagator
 355 during the highlighted part of the pulse sequence in Fig. 3b. **For convenience,**
 356 it is written as a product of individual propagators:

$$\begin{aligned}
 \hat{\mathcal{P}}_{tot}(t_{HF,1}, t_{up}, t_{relax}, t_{down}, t_{HF,2}) &= \hat{\mathcal{P}}^{HF,2}(t_{HF,2}) \cdot \hat{\mathcal{P}}^{down}(t_{down}) \cdot \hat{\mathcal{P}}^{LF}(t_{relax}) \cdot \\
 &\quad \hat{\mathcal{P}}^{up}(t_{up}) \cdot \hat{\mathcal{P}}^{HF,1}(t_{HF,1}),
 \end{aligned}
 \tag{28}$$

357 where $\hat{\mathcal{P}}^{HF,1}$ and $\hat{\mathcal{P}}^{HF,2}$ are the propagators calculated at high field, respec-
 358 tively before and after shuttling, $\hat{\mathcal{P}}^{LF}$ is the propagator calculated at the
 359 low field position and $\hat{\mathcal{P}}^{up}$ (respectively $\hat{\mathcal{P}}^{down}$) is the propagator calculated
 360 during the motion up (respectively down) from the high-field to the low-
 361 field position (respectively from the low-field to the high-field position). The
 362 propagators for constant-field positions (*i.e.* $\hat{\mathcal{P}}^{HF,1}$, $\hat{\mathcal{P}}^{LF}$ and $\hat{\mathcal{P}}^{HF,2}$) are cal-
 363 culated using Eq. 21 and the relaxation matrix calculated at high field ($\hat{\mathcal{R}}_{HF}$)
 364 and low field ($\hat{\mathcal{R}}_{LF}$):

$$\begin{aligned}
 \hat{\mathcal{P}}^{HF,i}(t_{HF,i}) &= e^{-t_{HF,i}\hat{\mathcal{R}}_{HF}}, \\
 \hat{\mathcal{P}}^{LF}(t_{relax}) &= e^{-t_{relax}\hat{\mathcal{R}}_{LF}}.
 \end{aligned}
 \tag{29}$$

365 The simulation of the transfers through the magnetic field gradient is per-
 366 formed by subdividing the experiment into intervals of few milli-seconds δt
 367 that still fulfill the conditions of Redfield theory. In order to stay in the
 368 Redfield hypothesis, δt must be large compared to the correlation time of
 369 the system to extend the integration to infinity in Eq. 5. In addition, δt must
 370 be sufficiently small in order to perform a discretization of the integral over
 371 the full sample trajectory. In the case of high-resolution relaxometry with a
 372 sample traveling at $\approx 10 \text{ m.s}^{-1}$ over at most 1 m, we considered a δt of 1 ms,
 373 which corresponds, at most, to a change of about 10 % of the magnetic field
 374 between two consecutive steps. The propagators $d\hat{\mathcal{P}}(\delta t, z(t))$ for these small
 375 steps are obtained following Eq. 21:

$$d\hat{\mathcal{P}}(\delta t, z(t)) = e^{-\delta t \hat{\mathcal{R}}(z(t))}, \quad (30)$$

376 where $\hat{\mathcal{R}}(z(t))$ is the relaxation matrix evaluated at the position $z(t)$ along
 377 the bore of the magnet and characterized by its magnetic field (note: the field
 378 profile can be mapped using a gaussmeter). The experimental field profile is
 379 fitted to a polynomial expansion in ICARUS. Each propagator $d\hat{\mathcal{P}}(\delta t, z(t))$
 380 is field dependent due to the field dependence of the relaxation matrix. The
 381 propagator for the motions up to and down from the position z_{relax} are defined
 382 as the products of the infinitesimal propagators $d\hat{\mathcal{P}}$:

$$\begin{aligned}
 \hat{\mathcal{P}}^{\text{up}} &= \prod_{n=0}^{n_{\text{max}}^{\text{up}}} d\hat{\mathcal{P}}^{\text{up}}(\delta t, (z(n \times \delta t))), \\
 \hat{\mathcal{P}}^{\text{down}} &= \prod_{n=0}^{n_{\text{max}}^{\text{down}}} d\hat{\mathcal{P}}^{\text{down}}(\delta t, (z(n \times \delta t))),
 \end{aligned} \quad (31)$$

383 where $n_{\text{max}}^{\text{up}}$ (respectively $n_{\text{max}}^{\text{down}}$) is defined by $t_{\text{transfer}}^{\text{up}} = n_{\text{max}} \times \delta t$ (respectively
 384 $t_{\text{transfer}}^{\text{down}} = n_{\text{max}} \times \delta t$) with $t_{\text{transfer}}^{\text{up}}$ (respectively $t_{\text{transfer}}^{\text{down}}$) the delay of transfer
 385 to the top (respectively down) position. In these calculations, the relaxation
 386 matrix is derived using the analytical expression obtained from REDKITE, a
 387 model of motions and a set of parameters of dynamics.

388 The expectation value for the operator of interest at the end of the full re-
 389 laxation period (delays at high field and low field as well as the two transfers
 390 in between) can then be extracted from the calculated propagator for each
 391 relaxation delay. The simulated decay as a function of the relaxation time

392 is fitted with a mono-exponential decay function with an effective longitudi-
 393 nal relaxation rate R_{sim} (Table 1 sums up our nomenclature for the different
 394 calculated and measured relaxometry relaxation rates). All relaxation path-
 395 ways are active during the transfers between high and low-field positions.
 396 The initial density operator is partially projected onto the eigenvectors of
 397 the relaxation matrix (relaxation modes) of lowest eigenvalues. Thus, the
 398 simulated decay rate R_{sim} is *a priori* lower than the pure longitudinal relax-
 399 ation rate R_{calc} calculated using the parameters of dynamics. We define the
 400 correction factor for each relaxometry experiment as the ratio between these
 401 two rates for an experiment j (corresponding to a specific low field $B_{LF}^{(j)}$) and
 402 a residue i :

$$\mathcal{C}(\mathcal{E}_j, B_{LF}^{(j)}, \mathcal{D}_i) = \frac{R_{calc}(B_{LF}^{(j)}, \mathcal{D}_i)}{R_{sim}(\mathcal{E}_j, B_{LF}^{(j)}, \mathcal{D}_i)}, \quad (32)$$

403 where \mathcal{E}_j are the experimental parameters (shuttling times and relaxation
 404 delays), and \mathcal{D}_i are the parameters of dynamics. The correction factor is
 405 applied to each corresponding measured relaxometry data $R_{meas}(\mathcal{E}_j, B_{LF}^{(j)})$:

$$R_{corr}(\mathcal{E}_j, B_{LF}^{(j)}) = \mathcal{C}(\mathcal{E}_j, B_{LF}^{(j)}, \mathcal{D}_i) \times R_{meas}(\mathcal{E}_j, B_{LF}^{(j)}). \quad (33)$$

406 The correction is performed iteratively (Fig. 4). The set of parameters \mathcal{D}_i
 407 for the first iteration is obtained from the analysis of the accurate relaxation
 408 rates, *i.e.* measured with the use of pulses, typically on high-field magnets.
 409 Then corrected relaxometry relaxation rates are analyzed alongside high-
 410 field relaxation rates. A new set of parameters of dynamics is extracted from
 411 this ensemble of relaxation rates. In the next iteration, these parameters
 412 of dynamics are used to simulate the experiment and compute improved
 413 corrections of experimental rates to estimate the accurate low-field relaxation
 414 rates. This is repeated until the correction factors converge. The final set
 415 of high-field and corrected relaxometry relaxation rates can then be used
 416 to extract the distribution of the parameters of local motions in a Markov-
 417 Chain Monte-Carlo (MCMC) procedure and thus evaluate the median value
 418 and uncertainty of these parameters (see below).

419 3.2.2. Compiling expressions in the *FunctionsFile.py* script

420 Information about the relaxation properties of the spin system are con-
 421 tained in an independent script called *FunctionsFile* with expressions of the
 422 relaxation rates (and their derivatives if required) and the relaxation ma-
 423 trix in the considered basis. The *FunctionsFile* can be edited and adapted

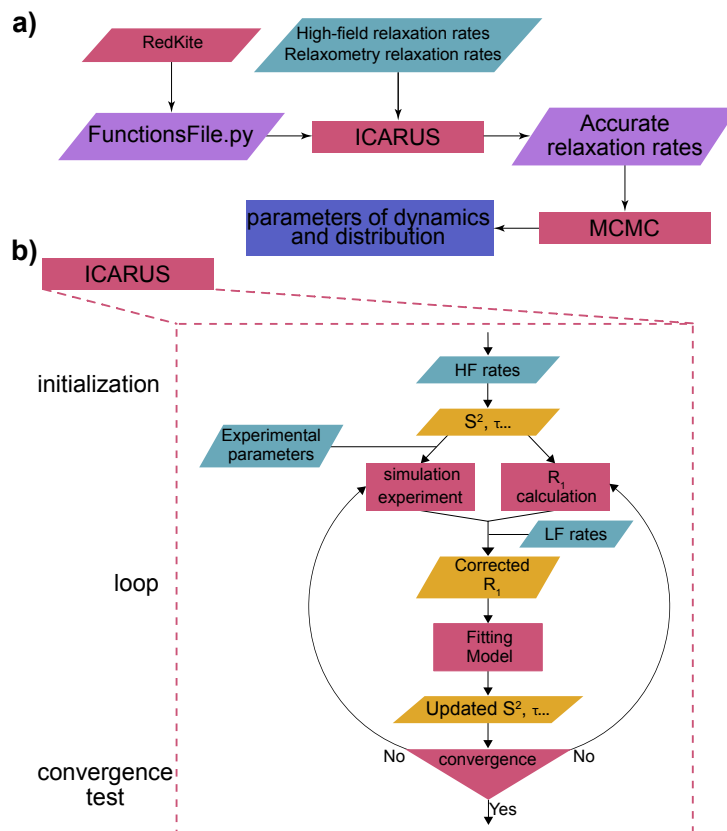


Figure 4: Flow chart for the analysis of high-resolution relaxometry data with ICARUS. **a)** After a FunctionsFile has been obtained from REDKITE, ICARUS can be run, using, among other inputs, relaxation rates recorded on standard high-field spectrometers and the high-resolution relaxometry data. Accurate relaxometry relaxation rates are obtained, and a Markov-Chain Monte-Carlo (MCMC) analysis of these corrected rates and high-field relaxation rates leads to values of parameters describing the dynamics of the system and their distribution. **b)** Flow chart of the ICARUS procedure. Accurate high-field (HF) relaxation rates are used to obtain an initial set of parameters for the dynamics of the system. These parameters are used to simulate the high-resolution relaxometry experiments (using the same experimental set up, *i.e.* shuttling time, delays, magnetic fields) from which biased simulated R_1 are extracted, and also to calculate the accurate expected R_1 . The ratios of these two calculated rates are called correction factors. The product of experimental decay rates and correction factors are corrected experimental low field (LF) relaxometry relaxation rates. Together with the high-field relaxation data, the corrected rates are used to determine a new set of parameters of dynamics, further used in the next correction iteration. Convergence is not evaluated within ICARUS and the number of iterations remains a choice of the user. However, we recommend to verify the convergence of the correction factors, as these ones are essential in the determination of the final parameters of the dynamics. Typically three or four iterations are sufficient.

Table 1: Nomenclature for the relaxometry relaxation rate labels and parameters determining their values. $\{\mathcal{E}_j\}$ are the experimental parameters for experiment j , $B_{\text{LF}}^{(j)}$ is the low field chosen for relaxation and \mathcal{D}_i are the parameters of the spectral density function used to describe the dynamics of residue i .

Label	Parameters	Description
R_{sim}	$\mathcal{E}_j, B_{\text{LF}}^{(j)}$ and \mathcal{D}_i	Relaxation rate extracted from the fitting of the simulated polarization decay
R_{calc}	$B_{\text{LF}}^{(j)}$ and \mathcal{D}_i	Relaxation rate calculated from the parameters of dynamics
R_{meas}	\mathcal{E}_j and $B_{\text{LF}}^{(j)}$	Measured relaxation decay rate
R_{corr}	$\mathcal{E}_j, B_{\text{LF}}^{(j)}$ and \mathcal{D}_i	Corrected relaxation decay rate

424 to the spin system under investigation. REDKITE outputs first need to be
 425 converted from MATHEMATICA to PYTHON format and compiled in this
 426 FunctionsFile.py script.

427 This task is performed by the RedKite2ICARUS.py program. Briefly, it takes
 428 as input all the output files from REDKITE (Section 3.1) and asks for vari-
 429 ables names (the ones that have to be fitted, usually parameters defining
 430 the spectral density function) and the ones that characterize the system and
 431 are not fitted (e.g., CSA tensors). It is also possible to set the CSA as a
 432 fitted variable. In the case where the overall diffusion frame is asymmetric,
 433 ICARUS requires a file containing the orientations of internuclear vectors in
 434 the anisotropic diffusion frame. Creating such a file has been implemented
 435 in RedKite2ICARUS.

436 3.2.3. Fitting parameters of the model of motion to relaxation rates

437 The program ICARUS (Iterative Correction for the Analysis of Relax-
 438 ation Under Shuttling) [17, 26] has been entirely written in PYTHON (version
 439 3.5). The detailed description on how to use ICARUS has been already pub-
 440 lished elsewhere [26]. The key parts of the code are the fitting of parameters
 441 of a user-defined model of motion using accurate (generally high field) re-
 442 laxation rates and corrected relaxometry rates as experimental constraints,

443 as well as the simulation of the experiments (as detailed in Section 3.2.1).
444 Fitting the parameters of the model relies on the *basin-hopping* function im-
445 plemented in the *scipy.optimize* PYTHON library with the L-BFGS-B method
446 [45] for χ^2 minimization:

$$\chi^2 = \sum_i \frac{(R_{\text{model},i} - R_{\text{exp},i})^2}{\sigma_{\text{exp},i}^2}, \quad (34)$$

447 where $R_{\text{model},i}$ are the calculated relaxation rates and $R_{\text{exp},i}$ are the measured
448 relaxation rates with experimental error $\sigma_{\text{exp},i}$.

449 Bounds of the dynamics parameters are provided by the user in the GUI.
450 The *basin-hopping* function allows the use of first derivatives of the relax-
451 ation rates in the fitting (provided in the FunctionsFile as explained above),
452 usually leading to faster minimization. An additional minimization based on
453 a grid search has been implemented in order to avoid local minimum traps.
454 This step is time-consuming and optional.

455 The core of the code does not contain information about a particular spin
456 system nor experimental set up, such that the usage of ICARUS can be
457 extended to any situation (spin system or model of motion). Data and ex-
458 perimental set up are loaded as separate text files using the GUI, and all
459 analytical expressions of relaxation rates are contained in the independent
460 FunctionsFile script.

461 3.2.4. ICARUS output and MCMC

462 The outputs of ICARUS have already been described [26]. Fig. 5 shows
463 selected figures created by ICARUS. Briefly, output figures consist of the fit
464 of the stray field gradient (Fig. 5a), profiles of the relaxation rates (accu-
465 rate, calculated, and corrected in the case of relaxometry data) at each field
466 throughout the protein sequence (Fig. 5b, c, d), fits of all the relaxation rates
467 for each residue (Fig. 5e, f), bar plots of fitted parameters (Fig. 5g). Several
468 text files are created which contain corrected relaxometry relaxation rates,
469 the set of fitted parameters after the fit of the accurate relaxation rates only,
470 and of the whole data set (accurate and corrected relaxometry data) as well
471 as the correction factors after each iteration of ICARUS. Finally, scripts are
472 also created. One allows the user to calculate all the defined relaxation rates
473 and the relaxation matrix using the final fitted parameters with the use of a
474 GUI where the magnetic field and residue number of interest have to be set.
475 The other scripts are created only if a PDB ID for the protein of interest

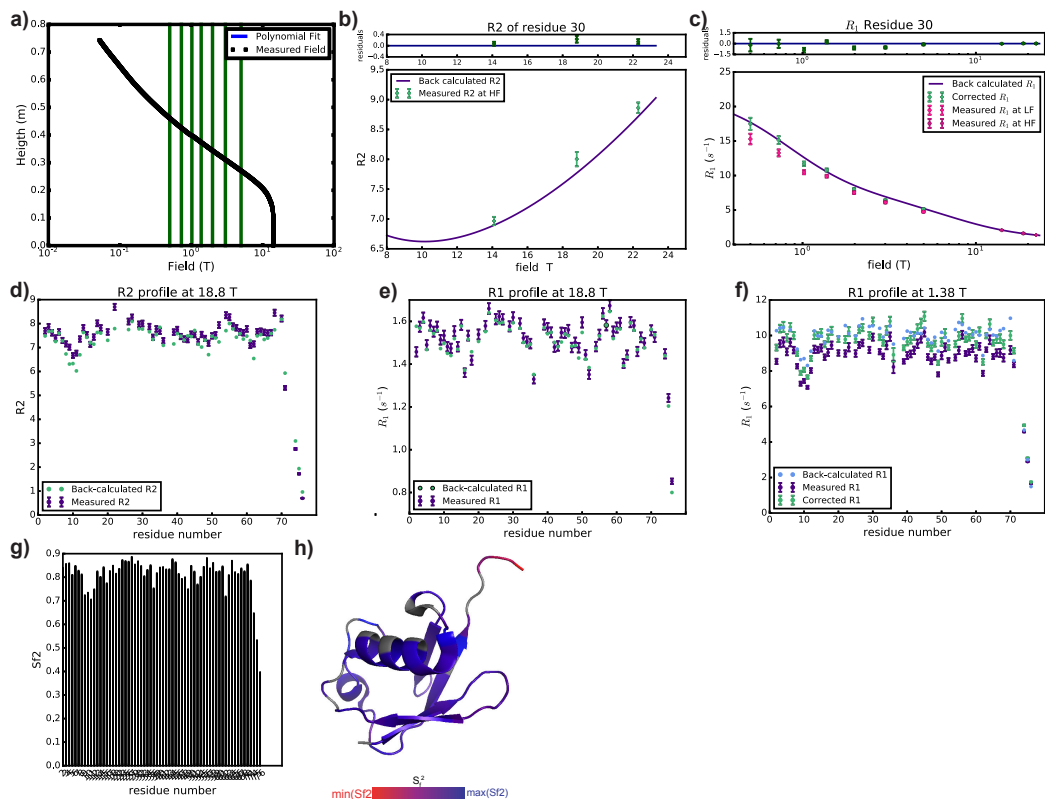


Figure 5: Outputs created by ICARUS for the study of motions of amide backbone ^{15}N of Ubiquitin. **a)** Fit of the magnetic field in the spectrometer. The vertical green lines show the magnetic fields at which relaxometry measurements were performed. Checking the quality of this fit is important in order to make sure magnetic fields will be calculated correctly for each position of the sample during its trajectories. **b)** and **c)** Fit of the nitrogen-15 transverse and longitudinal relaxation rates for the residue Ile-30. **d)** Transverse and **e)** longitudinal nitrogen-15 relaxation rates measured at 18.8 T. Measured and calculated relaxation rates using the final fitted parameters are shown in purple and green respectively. **f)** Profile of the longitudinal relaxometry nitrogen-15 relaxation rate at ≈ 1.38 T. Measured, corrected and calculated rates using the final set of fitted parameters are shown in purple, light green and dark green respectively. **g)** Evolution of the order parameter S_f^2 throughout the sequence (residues for which no data are provided are not displayed in this bar plot). **h)** Color-coding of the Ubiquitin structure (PDB ID: 1D3Z) according to the final fitted values of the order parameter S_f^2 . Residues for which no data are provided are shown in grey.

476 has been provided in the GUI, and are meant to be run in PYMOL in order
477 to color the structure according to the final set of fitted parameters (order
478 parameters, correlation times, etc...) and the final χ^2 (Eq. 34) to facilitate
479 the visualisation of the results over the protein structure (one file is created
480 for each of these parameters). An example is shown in Fig. 5h.

481 In order to provide a better analysis of the dynamics, a Markov-Chain Monte-
482 Carlo (MCMC) analysis of accurate and corrected relaxometry relaxation
483 rates should be performed. We have written a script that directly reads
484 ICARUS output folders to perform an MCMC using the *emcee* PYTHON li-
485 brary [46]. The MCMC analysis provides a better error evaluation of the
486 parameters of dynamics as well as potential correlations between them. A
487 README file explaining how to use the MCMC program is provided with
488 the script.

489 Overall, the REDKITE-ICARUS suite is intended to allow for an efficient
490 (a complete analysis of ^{15}N relaxometry data on Ubiquitin can be obtained
491 within two hours on a standard laptop computer) and highly flexible (it
492 can be extended to broad range of spin systems, with all types of model
493 of motions and for most commonly measured relaxation rates) analysis of
494 high-resolution relaxometry data. REDKITE and RedKite2ICARUS create
495 the scaffold (FunctionsFile) that is used by ICARUS. The use of ICARUS is
496 convenient with a simple graphical user interface. After the correction of the
497 relaxometry relaxation rate, a final Markov-Chain Monte-Carlo analysis is
498 performed by a script that reads directly ICARUS output folders (Fig. 4a).

499 4. Application to $\{^{13}\text{C}^1\text{H}^2\text{H}_2\}$ -methyl groups using HRR and 2F- 500 NMR

501 Motions of protein side-chains are important for their function. These
502 motions have been investigated thanks to NMR methodological development
503 and selective labeling strategies based on the clever use of metabolic path-
504 ways [47, 48, 49]. The averaging of the dipolar interactions arising from their
505 fast rotation confers favourable relaxation properties to methyl groups. They
506 make good candidates for the study of side-chain motions, in particular in
507 the hydrophobic core of proteins where they constitute an entropy reservoir
508 [50, 51], or at protein-protein and protein-ligand binding interfaces where
509 their motions can allow a re-modeling for a better complementary interac-
510 tion with the binding partner. In this context, we have recently performed
511 a detailed analysis of the motions of isoleucine- δ_1 methyl-group on the se-

512 lectively labeled protein U-[²H, ¹⁵N], Ile- δ_1 [¹³C²H₂¹H]-Ubiquitin with the use
 513 of HRR and relaxation rates recorded using conventional high-field magnets
 514 [25]. In this section, the combined REDKITE and ICARUS analysis of HRR
 515 in U-[²H, ¹⁵N], Ile- δ_1 [¹³C²H₂¹H]-Ubiquitin is presented.

516 4.1. Theoretical framework for the dynamics of methyl group

517 4.1.1. Model of correlation function

518 Different models of correlation function for a wide variety of molecular
 519 systems have been suggested in the past [43, 52, 53, 54, 55, 56, 57, 58]. In
 520 our analysis of high field and relaxometry relaxation rates on {¹³C¹H²H₂}
 521 methyl group of Ubiquitin, the data recorded at low fields (lower than 5 T)
 522 allowed a better characterization of the complexity of motions that can occur
 523 in a methyl-bearing side-chain, in particular χ_1/χ_2 rotameric transitions in
 524 isoleucine residues on nanosecond timescales [25]. The analysis was based
 525 on the Extended Model Free (EMF) description of the CC bond motions.
 526 Assuming (i) isotropic tumbling of the protein characterized by a correla-
 527 tion time τ_c , (ii) EMF for CC bonds motions, (iii) perfect tetrahedral sym-
 528 metry for the methyl group with a characteristic correlation time for the
 529 methyl group rotation τ_{met} associated to an order parameter $S_{met}^2(\theta_{i,j})$ [59]
 530 and (iv) statistical independence between methyl group rotation, motions of
 531 the methyl group axis and overall rotational diffusion, the correlation func-
 532 tion can be modeled by:

$$C_{i,j}^{met}(t) = C_g(t)C_{axis}(t)C_{rot}^{i,j}(t), \quad (35)$$

533 where:

$$\begin{aligned} C_g(t) &= e^{-t/\tau_c}, \\ C_{axis}(t) &= S^2 + (1 - S_f^2)e^{-t/\tau_f} + S_f^2(1 - S_s^2)e^{-t/\tau_s}, \\ C_{rot}^{i,j}(t) &= S_{met}^2(\theta_{i,j}) + (\mathcal{P}_2(\cos \theta_{i,j}) - S_{met}^2(\theta_{i,j})) e^{-t/\tau_{met}}, \end{aligned} \quad (36)$$

534 with $S_{met}^2(\theta_{i,j}) = \mathcal{P}_2(\cos \theta_i)\mathcal{P}_2(\cos \theta_j)$ and \mathcal{P}_2 is the second order Legendre
 535 polynomial function, $\mathcal{P}_2(x) = (3x^2 - 1)/2$, θ_k is the angle between the princi-
 536 pal axis of an axially symmetric interaction \mathbf{k} vector and the CC-axis (methyl
 537 group symmetry axis) and $\theta_{i,j}$ the angle between the principal axes of two
 538 (possibly identical) axially symmetric interactions \mathbf{i} and \mathbf{j} . The order param-
 539 eters S_f^2 and S_s^2 characterize motions of the system frame and are associated
 540 with the correlation times τ_f and τ_s , respectively. The overall order param-
 541 eter is defined as $S^2 = S_f^2 S_s^2$. The value of the angles θ_k and $\theta_{i,j}$ is constrained

542 by the geometry of the spin system. The corresponding spectral density
 543 function is:

$$\begin{aligned}
 \mathcal{J}_{i,j}(\omega) = \frac{1}{5} & \left[S_{met}^2(\theta_{i,j}) \left(S_f^2 S_s^2 \frac{\tau_c}{1 + (\omega\tau_c)^2} + (1 - S_f^2) \frac{\tau'_f}{1 + (\omega\tau'_f)^2} + \right. \right. \\
 & \left. \left. S_f^2 (1 - S_s^2) \frac{\tau'_s}{1 + (\omega\tau'_s)^2} \right) + (\mathcal{P}_2 \cos(\theta_{i,j}) - S_{met}^2(\theta_{i,j})) \times \right. \\
 & \left(S_f^2 S_s^2 \frac{\tau'_{met}}{1 + (\omega\tau'_{met})^2} + (1 - S_f^2) \frac{\tau''_f}{1 + (\omega\tau''_f)^2} + \right. \\
 & \left. \left. S_f^2 (1 - S_s^2) \frac{\tau''_s}{1 + (\omega\tau''_s)^2} \right) \right], \tag{37}
 \end{aligned}$$

544 where $\tau_a'^{-1} = \tau_a^{-1} + \tau_c^{-1}$ and $\tau_a''^{-1} = \tau_a^{-1} + \tau_c^{-1} + \tau_{met}^{-1}$.
 545 In the following, \mathcal{J}_{AB} will be used to denote the dipole-dipole auto-correlation
 546 between nuclei A and B, \mathcal{J}_A for the CSA auto-correlation of nucleus A,
 547 $\mathcal{J}_{AB,CD}$ for the dipole-dipole/dipole-dipole cross-correlation between the spin
 548 pairs AB and CD, $\mathcal{J}_{A,BC}$ for the cross-correlation between the CSA of nucleus
 549 A and the dipole-dipole interaction between nuclei B and C. Finally, the index
 550 \mathcal{Q} will be used to denote the quadrupolar interactions. These notations follow
 551 conventions proposed by Werbelow and Grant [60].

552 As detailed bellow, in our treatment of the relaxometry data, the effects of
 553 the surrounding deuterium nuclei arising from the labelling of the protein
 554 have to be considered. These have been taken into account by adding a
 555 single additional deuterium nucleus in the spin system. For simplicity, while
 556 we consider the additional dipolar contributions to relaxation rates of the
 557 $\{^{13}\text{C}^1\text{H}^2\text{H}_2\}$ spin system, we do not include this additional nucleus in our
 558 basis. We approximated the spectral density function for the correlations
 559 involving this vicinal deuterium D_{vic} to be described by Eq. 37, although it
 560 is not part of the methyl group.

561 4.1.2. Relaxation rates

562 In our analysis of high-field and relaxometry relaxation rates on $\{^{13}\text{C}^1\text{H}^2\text{H}_2\}$ -
 563 methyl groups of Ubiquitin, longitudinal and transverse carbon-13 autore-
 564 laxation rates, longitudinal proton autorelaxation rates and dipolar cross-
 565 relaxation rates were used. Dipolar relaxation with an effective vicinal deu-
 566 terium was considered. The set-up of REDKITE for such a spin system is
 567 detailed in Supplementary Materials. The contribution of the proton CSA

568 to relaxation is expected to be negligible [61], and is not considered in the
569 following. The CSA tensor of the carbon-13 nucleus is assumed to be sym-
570 metric and aligned with the CC bond. Expressions of the relaxation rates
571 are given in the following equations:

$$\begin{aligned}
R_1(^{13}\text{C}) &= \frac{2}{3} \Delta\sigma_C^2 \omega_C^2 \mathcal{J}_C(\omega_C) \\
&\quad + \frac{1}{2} d_{\text{CH}}^2 (\mathcal{J}_{\text{CH}}(\omega_C - \omega_{\text{H}}) + 3\mathcal{J}_{\text{CH}}(\omega_C) + 6\mathcal{J}_{\text{CH}}(\omega_C + \omega_{\text{H}})) \\
&\quad + \frac{8}{3} d_{\text{CD}}^2 (\mathcal{J}_{\text{CD}}(\omega_C - \omega_{\text{D}}) + 3\mathcal{J}_{\text{CD}}(\omega_C) + 6\mathcal{J}_{\text{CD}}(\omega_C + \omega_{\text{D}})) \\
&\quad + \frac{4}{3} d_{\text{CD}_{\text{vic}}}^2 (\mathcal{J}_{\text{CD}_{\text{vic}}}(\omega_C - \omega_{\text{D}}) + 3\mathcal{J}_{\text{CD}_{\text{vic}}}(\omega_C) + 6\mathcal{J}_{\text{CD}_{\text{vic}}}(\omega_C + \omega_{\text{D}})), \\
R_2(^{13}\text{C}) &= \frac{1}{9} \Delta\sigma_C^2 \omega_C^2 (4\mathcal{J}_C(0) + 3\mathcal{J}_C(\omega_C)) \\
&\quad + \frac{1}{4} d_{\text{CH}}^2 (4\mathcal{J}_{\text{CH}}(0) + \mathcal{J}_{\text{CH}}(\omega_C - \omega_{\text{H}}) + 3\mathcal{J}_{\text{CH}}(\omega_C) + 6\mathcal{J}_{\text{CH}}(\omega_{\text{H}}) \\
&\quad + 6\mathcal{J}_{\text{CH}}(\omega_C + \omega_{\text{H}})) \\
&\quad + \frac{4}{3} d_{\text{CD}}^2 (4\mathcal{J}_{\text{CD}}(0) + \mathcal{J}_{\text{CD}}(\omega_C - \omega_{\text{D}}) + 3\mathcal{J}_{\text{CD}}(\omega_C) + 6\mathcal{J}_{\text{CD}}(\omega_{\text{D}}) \\
&\quad + 6\mathcal{J}_{\text{CD}}(\omega_C + \omega_{\text{D}})) \\
&\quad + \frac{2}{3} d_{\text{CD}_{\text{vic}}}^2 (4\mathcal{J}_{\text{CD}_{\text{vic}}}(0) + \mathcal{J}_{\text{CD}_{\text{vic}}}(\omega_C - \omega_{\text{D}}) + 3\mathcal{J}_{\text{CD}_{\text{vic}}}(\omega_C) \\
&\quad + 6\mathcal{J}_{\text{CD}_{\text{vic}}}(\omega_{\text{D}}) + 6\mathcal{J}_{\text{CD}_{\text{vic}}}(\omega_C + \omega_{\text{D}})), \\
R_1(^1\text{H}) &= \frac{1}{2} d_{\text{CH}}^2 (\mathcal{J}_{\text{CH}}(\omega_C - \omega_{\text{H}}) + 3\mathcal{J}_{\text{CH}}(\omega_{\text{H}}) + 6\mathcal{J}_{\text{CH}}(\omega_C + \omega_{\text{H}})) \\
&\quad + \frac{8}{3} d_{\text{HD}}^2 (\mathcal{J}_{\text{HD}}(\omega_{\text{D}} - \omega_{\text{H}}) + 3\mathcal{J}_{\text{HD}}(\omega_{\text{H}}) + 6\mathcal{J}_{\text{HD}}(\omega_{\text{D}} + \omega_{\text{H}})) \\
&\quad + \frac{4}{3} d_{\text{HD}_{\text{vic}}}^2 (\mathcal{J}_{\text{HD}_{\text{vic}}}(\omega_{\text{D}} - \omega_{\text{H}}) + 3\mathcal{J}_{\text{HD}_{\text{vic}}}(\omega_{\text{H}}) + 6\mathcal{J}_{\text{HD}_{\text{vic}}}(\omega_{\text{D}} + \omega_{\text{H}})), \\
\sigma_{\text{CH}} &= \frac{1}{2} d_{\text{CH}}^2 (-\mathcal{J}_{\text{CH}}(\omega_C - \omega_{\text{H}}) + 6\mathcal{J}_{\text{CH}}(\omega_C + \omega_{\text{H}})),
\end{aligned} \tag{38}$$

572 where d_{AB} is the dipolar coefficient between atoms A and B and equals
573 $-(\mu_0 \hbar \gamma_A \gamma_B) / (4\pi r_{AB}^3)$ with μ_0 the permeability of free space, \hbar the Planck's
574 constant divided by 2π , γ_X the gyromagnetic ratio of nucleus X and r_{AB}
575 the internuclear distance between nuclei A and B , $\Delta\sigma_C$ is the chemical shift
576 anisotropy of the carbon-13 nucleus and $\omega_X = -\gamma_X B_0$ is the Larmor fre-

577 quency for the nuclei X at a magnetic field B_0 . The geometry of the methyl
 578 group was assumed to be tetrahedral with $r_{\text{CH}} = r_{\text{CD}} = 111.5$ pm leading
 579 to $r_{\text{HD}} = 182$ pm. The distance $r_{\text{CD}_{\text{vic}}}$ is determined during the ICARUS
 580 analysis as described below.

581 *4.1.3. Relaxation matrix*

582 The secularized basis for the subspace that includes \hat{C}_z in a $\{^{13}\text{C}^1\text{H}^2\text{H}_2\}$ -
 583 methyl group contains 14 terms:

$$\mathcal{B}_{\text{secularized}} = \left\{ \frac{\hat{C}_z}{3\sqrt{3}}, \frac{\hat{H}_z}{3\sqrt{3}}, \frac{\hat{D}_{1,z}}{6\sqrt{2}}, \frac{\hat{D}_{2,z}}{6\sqrt{2}}, \frac{2\hat{C}_z\hat{H}_z}{3\sqrt{3}}, \frac{\hat{C}_z\hat{D}_{1,z}}{3\sqrt{3}}, \frac{\hat{C}_z\hat{D}_{2,z}}{3\sqrt{3}}, \frac{\sqrt{2}\hat{C}_z\hat{H}_z\hat{D}_{1,z}}{3}, \right. \\ \left. \frac{\sqrt{2}\hat{C}_z\hat{H}_z\hat{D}_{2,z}}{3}, \frac{\hat{C}_z\hat{D}_{1,z}\hat{D}_{2,z}}{2\sqrt{3}}, \frac{\hat{C}_z\hat{D}_1^+\hat{D}_2^-}{4\sqrt{3}}, \frac{\hat{C}_z\hat{D}_1^-\hat{D}_2^+}{4\sqrt{3}}, \right. \\ \left. \frac{3\hat{C}_z\hat{D}_{1,z}\hat{D}_{1,z} - 2\hat{C}_z}{3\sqrt{6}}, \frac{3\hat{C}_z\hat{D}_{2,z}\hat{D}_{2,z} - 2\hat{C}_z}{3\sqrt{6}} \right\}, \quad (39)$$

584 where C , H , D_1 and D_2 refer to the carbon, proton, deuterium 1 and deu-
 585 terium 2, respectively, as defined in the spin system in REDKITE. The deu-
 586 terium 1 and 2 are considered magnetically equivalent and can be exchanged
 587 by symmetry (see Fig. 7c for a visualisization of the geometry of the system).
 588 As shown below, the analysis of the relaxation properties of the $\{^{13}\text{C}^1\text{H}^2\text{H}_2\}$ -
 589 methyl groups of Ubiquitin during a relaxometry experiment can be per-
 590 formed with satisfactory accuracy in the subspace spanned by the three op-
 591 erators:

$$\mathcal{B}_{\text{reduced},3} = \left\{ \frac{\hat{C}_z}{3\sqrt{3}}, \frac{\hat{H}_z}{3\sqrt{3}}, \frac{2\hat{C}_z\hat{H}_z}{3\sqrt{3}} \right\}, \quad (40)$$

592 leading to the following relaxation matrix:

$$\mathcal{R}_3 = \begin{pmatrix} R_1(^{13}\text{C}) & \sigma_{\text{CH}} & \eta_z^{\text{C}} \\ \sigma_{\text{CH}} & R_1(^1\text{H}) & 0 \\ \eta_z^{\text{C}} & 0 & R_{\text{CH}} \end{pmatrix}, \quad (41)$$

593 where $R_1(^{13}\text{C})$, $R_1(^1\text{H})$ and σ_{CH} are defined above and:

$$\begin{aligned}
R_{\text{CH}} = & \frac{2}{3}\Delta\sigma_{\text{C}}^2\omega_{\text{C}}^2\mathcal{J}_{\text{C}}(\omega_{\text{C}}) + \frac{3}{2}d_{\text{CH}}^2(\mathcal{J}_{\text{CH}}(\omega_{\text{C}}) + \mathcal{J}_{\text{CH}}(\omega_{\text{H}})) \\
& + \frac{8}{3}d_{\text{CD}}^2(\mathcal{J}_{\text{CD}}(\omega_{\text{C}} - \omega_{\text{D}}) + 3\mathcal{J}_{\text{CD}}(\omega_{\text{C}}) + 6\mathcal{J}_{\text{CD}}(\omega_{\text{C}} + \omega_{\text{D}})) \\
& + \frac{8}{3}d_{\text{HD}}^2(\mathcal{J}_{\text{HD}}(\omega_{\text{H}} - \omega_{\text{D}}) + 3\mathcal{J}_{\text{HD}}(\omega_{\text{H}}) + 6\mathcal{J}_{\text{HD}}(\omega_{\text{H}} + \omega_{\text{D}})) \\
& + \frac{4}{3}d_{\text{CD,vic}}^2(\mathcal{J}_{\text{CD,vic}}(\omega_{\text{C}} - \omega_{\text{D}}) + 3\mathcal{J}_{\text{CD,vic}}(\omega_{\text{C}}) + 6\mathcal{J}_{\text{CD,vic}}(\omega_{\text{C}} + \omega_{\text{D}})) \\
& + \frac{4}{3}d_{\text{HD,vic}}^2(\mathcal{J}_{\text{HD,vic}}(\omega_{\text{H}} - \omega_{\text{D}}) + 3\mathcal{J}_{\text{HD,vic}}(\omega_{\text{H}}) + 6\mathcal{J}_{\text{HD,vic}}(\omega_{\text{H}} + \omega_{\text{D}})), \\
\eta_z^{\text{C}} = & -2\Delta\sigma_{\text{C}}\omega_{\text{C}}d_{\text{CH}}\mathcal{J}_{\text{C,CH}}(\omega_{\text{C}}).
\end{aligned} \tag{42}$$

594 The expression of the secularized relaxation matrix can be found in the Sup-
595 plementary Materials.

596 4.2. Analysis of several aspects of the relaxation in methyl groups

597 4.2.1. Size of the relaxation matrix

598 The ICARUS protocol aims at obtaining accurate estimates of low-field
599 relaxation rates by accounting for the effects of cross-relaxation on the longi-
600 tudinal relaxation decays during a high-resolution relaxometry experiment.
601 This estimate is based on the simulation of the relaxometry experiments,
602 where the sample travels through a broad range of magnetic fields. In order
603 to obtain a reliable description of relaxation over orders of magnitude of mag-
604 netic fields, simulations must use appropriate relaxation matrices as well as
605 expressions of relaxation rates, with accurate parameters for the amplitudes
606 of interactions and the description of the spectral density function. The full
607 Liouville space for a $\{^{13}\text{C}^1\text{H}^2\text{H}_2\}$ spin system is spanned by a large basis of
608 $(2 \times \frac{1}{2} + 1)^{2 \times n_{1/2}} \times (2 \times 1 + 1)^{2 \times n_1} = 1296$ spin terms, with $n_{1/2}$ and n_1 the num-
609 ber of spin-half and spin-one respectively (Fig. 6a). An efficient calculation
610 requires to minimize the size of the Liouville space where the evolution of
611 the density operator is calculated. We have reduced the size of the subspace
612 using the steps described in Section 3.1 for $^{15}\text{N}-^1\text{H}$ spin systems. First, we
613 have considered the subspace only spanned by zero-quantum coherences and
614 population operators (Fig. 6b). We then applied the secular approximation,
615 and calculated all cross-relaxation terms with the \hat{C}_z operator, in order to
616 keep only non zero terms, *i.e.* terms that cross-relax with \hat{C}_z , reducing the

617 size of the basis to 14 terms (Fig. 6d). Cross-relaxation and autorelaxation
618 rates in this 14-element basis have been calculated at the lowest and high-
619 est magnetic fields used during our HRR experiments, *i.e.* 0.33 T and 14.1 T,
620 using parameters obtained after a preliminary ICARUS analysis (for Ile-3)
621 performed using $\mathcal{B}_{reduced,3}$ (Eq. 40, Fig. 6e).
622 The inspection of these two relaxation matrices justifies the use of a basis
623 containing only 3 operators as cross-relaxation rates involving other operators
624 are either negligible (cross relaxation to an operator B can be neglected if the
625 ratio of the cross-relaxation rate from A to B to the auto-relaxation rate of A
626 is small) or involve an operator relaxing very fast compared to the \hat{C}_z opera-
627 tor (see the Supplementary Materials for the proof that cross-relaxation with
628 fast relaxing operator do not contribute to the polarization decay of slowly
629 relaxing operators). At both magnetic fields, the largest cross-relaxation rate
630 with the carbon-13 longitudinal polarization is the dipolar cross-relaxation
631 with the proton longitudinal polarization. At low magnetic field (0.33 T),
632 even a 2-operator basis $\{\frac{1}{3}\hat{C}_z, \frac{1}{3}\hat{H}_z\}$ would be sufficient to describe the relax-
633 ation properties of a $\{^{13}\text{C}^1\text{H}^2\text{H}_2\}$ -methyl group as cross-relaxation towards
634 other terms is either very small or towards fast-relaxing terms. However,
635 the subspace should include the two-spin order $2\hat{C}_z\hat{H}_z$ at high field (14.1 T).
636 Thus, high-resolution relaxometry experiments in $\{^{13}\text{C}^1\text{H}^2\text{H}_2\}$ -methyl groups
637 have been simulated in the small subspace spanned by the three operators
638 (\hat{C}_z , \hat{H}_z and $2\hat{C}_z\hat{H}_z$). This subspace was used throughout our analysis of
639 carbon-13 HRR in $\{^{13}\text{C}^1\text{H}^2\text{H}_2\}$ methyl groups.

640 4.2.2. Proton relaxation and surrounding deuterium

641 Proton longitudinal relaxation rates $R_1(^1\text{H})$ were measured at three mag-
642 netic fields (0.33, 14.1 and 18.8 T) using standard high-field magnets (18.8 T
643 and 14.1 T) and a 2F-NMR spectrometer operating at 14.1 T and 0.33 T
644 [21]. These rates were also calculated after an ICARUS analysis of high-
645 field and HRR rates considering intra-methyl group interactions only. The
646 predicted relaxation rates are systematically lower than those measured at
647 0.33 T, 14.1 T and 18.8 T (Fig. 7a, b). Thus, even if relaxation rates in a
648 $\{^{13}\text{C}^1\text{H}^2\text{H}_2\}$ -methyl group are dominated by the contributions of internal in-
649 teractions, another contribution to relaxation has to be taken into account to
650 describe proton relaxation. The differences between the measured and calcu-
651 lated $R_1(^1\text{H})$ rates were assigned to the effect of the neighbouring deuterium
652 nuclei.

653 Adding the dipolar interactions with surrounding deuterium nuclei leads to

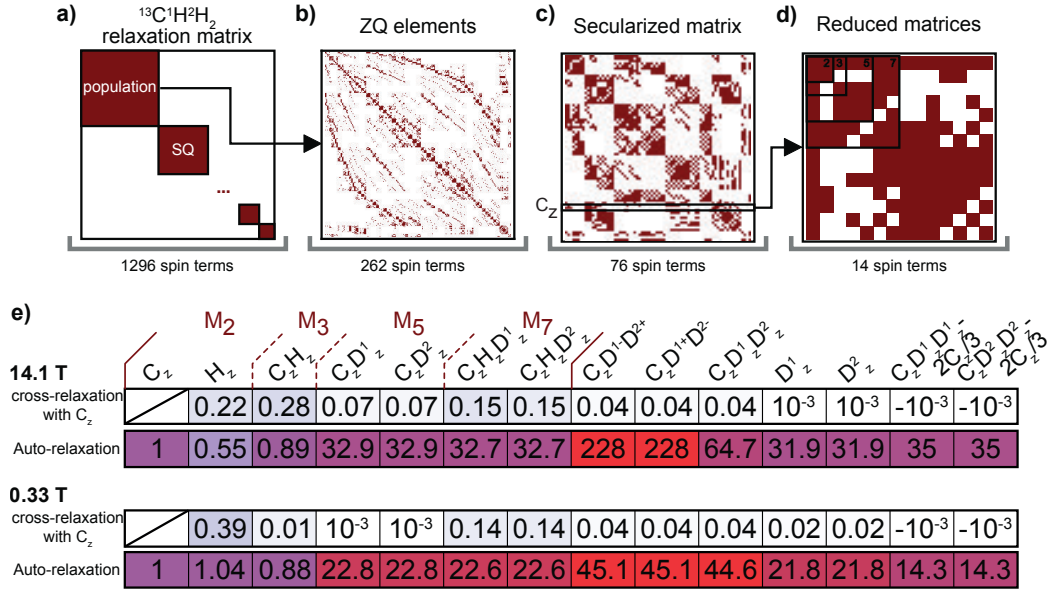


Figure 6: Relaxation matrix size-reduction in a $\{^{13}\text{C}^1\text{H}^2\text{H}_2\}$ -methyl group. **a)** Full relaxation matrix of a $\{^{13}\text{C}^1\text{H}^2\text{H}_2\}$ -methyl group. **b)** Relaxation matrix of the Zero-Quantum (ZQ) coherences and populations are selected. At this stage, the matrix has a 262x262 size. **c)** Secularized relaxation matrix containing 76 secular terms in the Zeeman interaction frame. The line corresponding to the operator of interest (\hat{C}_z) is highlighted. **d)** Relaxation matrix containing only terms cross-relaxing with the operator of interest (\hat{C}_z). Evaluating the cross-relaxation rates allows another level of size reduction. **e)** Numerical values of the diagonal terms of the relaxation matrix shown in d) (auto-relaxation, bottom row) and cross-relaxation rates with \hat{C}_z (top row) for the motional parameters of the $\delta 1$ methyl group of Ile-3 in U-[^2H , ^{15}N], Ile- $\delta 1$ [$^{13}\text{C}^2\text{H}_2^1\text{H}$]-Ubiquitin at 14.1 T and 0.33 T (reported in Ref. [25]). Relaxation rates are normalized to the auto-relaxation rate of \hat{C}_z at each magnetic field.

654 non-negligible contributions to relaxation to both the proton and the carbon-
655 13. The closest neighbouring deuterium nuclei are the $^2\text{H}\gamma_1$ and $^2\text{H}\gamma_2$ sites
656 of the isoleucine side-chain, but other deuterium nuclei may also be in close
657 proximity to the methyl group especially within the hydrophobic core of the
658 protein. The correlation function for the fluctuations of the corresponding
659 internuclear vectors are expected to vary. In particular, these interactions are
660 expected to be affected in different ways by the fast rotation of the methyl
661 group. We modeled the surrounding deuterium nuclei by a single deuterium
662 at an effective distance (Fig. 7c). The interaction of the proton and carbon-13
663 nuclei of the methyl group with this deuterium accounts for the interaction
664 with all the other deuterium nuclei of the protein. We used two adjustable
665 parameters to describe its position, defining its coordinates in the Carte-
666 sian axis system: the y- and z-coordinate were fitted while the x-coordinate
667 was fixed to 0. The position of the effective surrounding deuterium nucleus
668 is determined independently for each residue using proton relaxation rates
669 as well as all relaxation rates used in the ICARUS iterations (accurate and
670 corrected) and keeping the other parameters constant (*i.e.* the parameters
671 describing the dynamics). When fitting the parameters of the model during
672 further ICARUS analysis, the effective position of the surrounding deuterium
673 is kept constant. Introducing the contribution of the surrounding deuterium
674 and performing the whole ICARUS analysis again preserves the agreement
675 between the measured and calculated proton longitudinal relaxation rates
676 (Fig. 7a, b).

677 The surrounding deuterium has an effect on the correction factors (Fig. 7d)
678 which leads to differences of corrected HRR rates between 0 and 4 % (Fig. 7e).
679 Correction factors depend on the magnetic field and generally increase with
680 decreasing magnetic. It must be pointed out that non-monotonous changes
681 in the correction factors profiles in Fig. 7d are due to differences in shuttling
682 and waiting delays at low magnetic fields (Fig. S2).

683 The effective distances with the surrounding deuterium nucleus are close
684 to extracted distances from the NMR structure of Ubiquitin (Fig. 7f, PDB
685 1D3Z). The dipolar interaction between the methyl group and the effective
686 deuterium is included in the following iterations of the ICARUS analysis.

687 4.2.3. Convergence of the iterative correction

688 The number of iteration steps is expected to be dependent on the spin
689 system under study. In the case of the $\{^{13}\text{C}^1\text{H}^2\text{H}_2\}$ -spin system, the conver-
690 gence was reached after 2 iterations (Fig. 8a) for all residues except residue

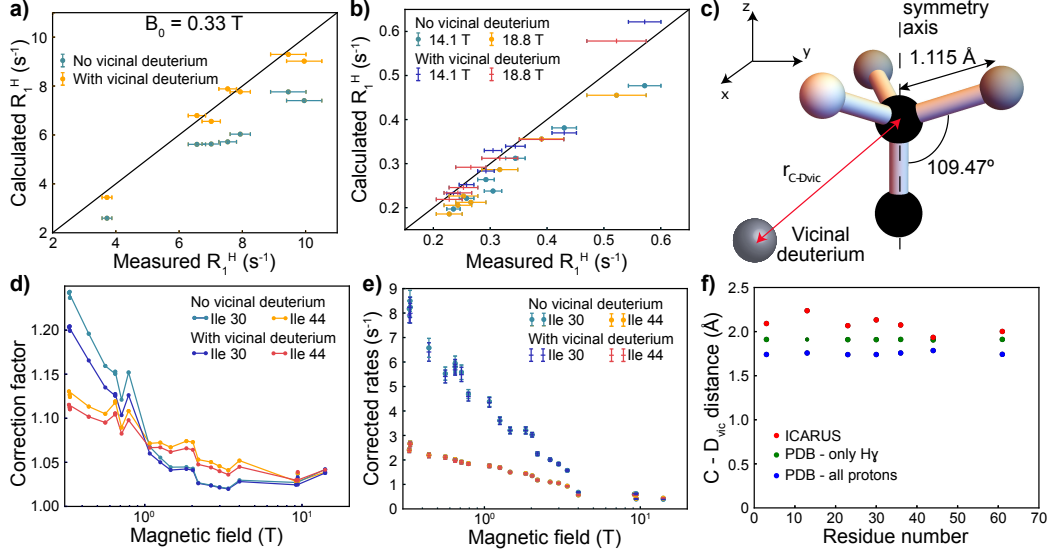


Figure 7: Including the effect of an effective vicinal deuterium nucleus on the analysis of high-resolution relaxometry data of U- $[^2\text{H}, ^{15}\text{N}]$, Ile- δ_1 [$^{13}\text{C}^2\text{H}_2^1\text{H}$]-Ubiquitin. **a)** Correlation plot of the calculated proton longitudinal relaxation rate R_1 at 0.33 T with (orange) and without (blue) including the effect of the vicinal deuterium, with the experimental R_1 at 0.33 T, for the seven isoleucines of Ubiquitin. The black line is shown as a guide for perfect equality between the two rates. **b)** Correlation plots of the calculated proton longitudinal relaxation rate R_1 at 14.1 T and 18.8 T with and without including the effect of the vicinal deuterium, with the experimental R_1 at 14.1 T and 18.8 T, for the seven isoleucines of Ubiquitin. The black line is shown as a guide for perfect equality between the two rates. **c)** Geometry of the methyl group and position of the effective neighbouring deuterium. The distance $r_{\text{C-D}_{\text{vic}}} = \sqrt{r_{\text{y,D}_{\text{vic}}}^2 + r_{\text{z,D}_{\text{vic}}}^2}$ is determined using additional relaxation rates as explained in the main text. **d)** Correction factors as a function of the magnetic field for Ile-30 and Ile-44 with and without an effective vicinal deuterium nucleus. **e)** Corrected relaxometry relaxation rates for Ile-30 and Ile-44 with and without including an effective vicinal deuterium nucleus. **f)** Comparison of the distance of the vicinal deuterium with the carbon-13 nucleus obtained from the analysis of proton relaxation (red, ICARUS) to the calculated distance to an effective deuterium nucleus that accounts for either only the $^2\text{H}\gamma_1$ and $^2\text{H}\gamma_2$ nuclei of the isoleucine residue (green) or all the hydrogens (blue) in the structure of Ubiquitin (PDB ID: 1D3Z). In these NMR derived structures, the distances were averaged over the 10 models present in the PDB file. In each model, the distance equals $r_{\text{C-D}_{\text{vic}}} = \left(\sum_i \frac{1}{d_i^6}\right)^{-1/6}$ with d_i the distance of the carbon-13 to proton i (excluding intra-methyl group proton).

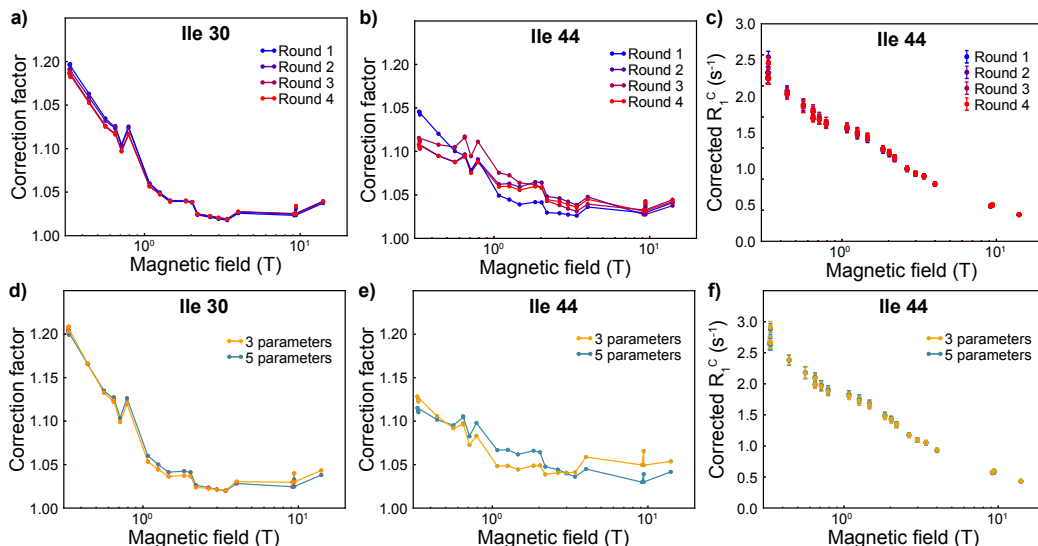


Figure 8: Evolution of the correction with the number of iterations of ICARUS and the selected model of motions. Correction factors as a function of the magnetic field for (a) Ile-30 and (b) Ile-44 after 1 to 4 rounds of ICARUS. (c) Evolution of the corrected relaxation rates of Ile-44 after 1 to 4 rounds of ICARUS. Correction factors as a function of the magnetic field for (d) Ile-30 and (e) Ile-44 using a model of spectral density function with 3 (Eq. 43, orange) or 5 (Eq. 37, blue) parameters to describe internal dynamics. (f) Corrected relaxation rates of Ile-44 obtained with a model with 3 (Eq. 43, orange) or 5 (Eq. 37, blue) parameters to describe internal dynamics.

691 44. Some slight instability in the convergence of the correction at low field
 692 is observed for this residue (Fig. 8b) but the amplitude of change (1-2 % at
 693 most) has a negligible effect on the values of the corrected relaxation rates
 694 (Fig. 8c).

695 4.2.4. Influence of the model of spectral density function on the correction

696 Different models can be used to describe the motions in a methyl group.
 697 Eq. 37 gives a rather complex description of the motion, but a simpler model
 698 can be tested by reducing the number of internal dynamics parameters to 3
 699 by only considering the global tumbling, the methyl-group rotation with one
 700 fitted correlation time and C-C axis motions with only one fitted correlation
 701 time and one order parameter. The spectral density function for this model

702 is:

$$\begin{aligned}
\mathcal{J}_{i,j}^{(3)}(\omega) = & \frac{1}{5} \left[S_{met}^2(\theta_{i,j}) \left(S^2 \frac{\tau_c}{1 + (\omega\tau_c)^2} + (1 - S^2) \frac{\tau'_{int}}{1 + (\omega\tau'_{int})^2} \right) \right. \\
& + (\mathcal{P}_2 \cos(\theta_{i,j}) - S_{met}^2(\theta_{i,j})) \left(S^2 \frac{\tau'_{met}}{1 + (\omega\tau'_{met})^2} \right. \\
& \left. \left. + (1 - S^2) \frac{\tau''_{int}}{1 + (\omega\tau''_{int})^2} \right) \right], \tag{43}
\end{aligned}$$

703 with the same definitions as above and where τ_{int} is an internal correlation
704 time for the motion of the C-C axis. Correction factors obtained for the two
705 spectral density functions are shown in Fig. 8d and e. They are identical
706 for Ile-30 where both models fit the experimental data well. In contrast, the
707 correction is slightly different for the two models of motion for Ile-44 (Fig. 8e),
708 where the 5-parameters model is in better agreement with the experiments.
709 Yet, the variation on the corrected rates is small (between 1 and 2 %, Fig. 8f)
710 with equally small effects on the analysis. The ICARUS analysis requires a
711 model that accounts for the overall changes of the spectral density function on
712 the range of frequencies probed during the experiments but it does not require
713 that the used model reproduces all subtle details of the spectral density
714 function: small variations of the value of the spectral density function at a
715 specific frequency have negligible effects on the correction.

716 *4.2.5. Scaling of the CSA/dipole-dipole cross-correlated cross-relaxation rates*

717 Our combined analysis of low-field longitudinal and high-field transverse
718 relaxation has allowed us to obtain the value of the CSA for each residue
719 in addition to parameters of internal motions, except for Ile-44 for which
720 chemical exchange prevented the analysis of the carbon-13 transverse relax-
721 ation rates [25]. In order to validate our analysis, a series of relaxation rates
722 were measured as detailed hereafter: accurate low field carbon longitudi-
723 nal relaxation rates [21] as well as high-field longitudinal CSA/dipole-dipole
724 (CSA/DD) cross-correlated cross-relaxation rates (cross-relaxation between
725 \hat{C}_z and $2\hat{C}_z\hat{H}_z$ referred to as η_z^C). These relaxation rates were not used during
726 the analysis of the relaxometry relaxation rates, but calculated using the set
727 of motional parameters obtained after correction of the relaxometry data.
728 The calculated longitudinal CSA/DD cross-relaxation rates were strongly
729 correlated to measurements at 14.1 T and 18.8 T but significantly overes-
730 timated (Fig. 9a). In order to have a better description of the CSA/DD

731 cross-correlation, a scaling factor was applied directly to this term in the
732 relaxation matrix. The scaling factor was calculated as the averaged inverse
733 correlation coefficient between the unscaled and measured η_z^C at 14.1 T and
734 18.8 T and equals 0.505. A number of hypothesis can be made to explain the
735 origin of the scaling factor: i) the carbon-13 CSA may be overestimated since
736 it is determined essentially from transverse relaxation rates, which may suffer
737 from small chemical exchange contributions; ii) the carbon-13 CSA may not
738 be perfectly alligned with the C-C bond; iii) the form of the spectral density
739 function may not describe correctly the motions of the methyl group; iv) the
740 amplitude of the carbon-13 CSA may be rotamer-dependent.

741 To understand the origin of this scaling factor, we also measured the car-
742 bon transverse CSA/DD cross-correlated cross-relaxation rates (η_{xy}^C). The
743 calculated relaxation rates correlate with the measurement, with an aver-
744 aged inverse correlation coefficient between the calculated and measured
745 η_{xy}^C at 14.1 T and 18.8 T of 0.629 (Supplementary Materials Fig. S3). The
746 discrepancy between the scaling factors of the longitudinal and transverse
747 CSA/DD cross-correlated cross-relaxation rates can not be accounted for
748 only from a miss-evaluation of the carbon-13 CSA (under our assumptions
749 of axially symmetry and perfect alignment allong the CC bond). Thus, it is
750 likely that the model of correlation function does not describe entirely the
751 complexity of the motions in the methyl group, and additional work toward
752 this direction has to be done. For example, transitions between rotamers
753 may be better modelled with instantateous jumps.

754 The analysis of the relaxometry relaxation data was performed again af-
755 ter applying the scaling factor to longitudinal CSA/DD relaxation rates.
756 As expected, the agreement between calculated and measured CSA/DD
757 cross-relaxation rates is significantly improved by the use of a scaling fac-
758 tor (Fig. 9a). Low-field correction factors are not sensitive to the scaling of
759 a CSA-dependent relaxation rate (Fig. 9b). At moderate and high field, the
760 effect is larger with a reduction of the correction by about 2% which has
761 limited impact on the analysis.

762 *4.3. Validation of the correction with the suppression of cross-relaxation path-* 763 *ways*

764 Using the recently developed 2F-NMR spectrometer [20, 19], we mea-
765 sured, among other relaxation rates, the longitudinal carbon-13 relaxation
766 rates at 0.33 T with suppression of cross-relaxation pathways [21]. The rates
767 of the seven isoleucines acquired at 0.33 T have been compared to mea-

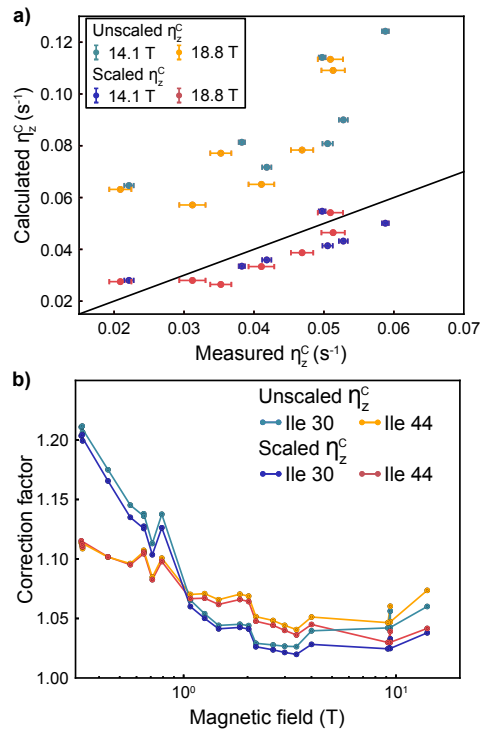


Figure 9: Scaling the CSA/DD cross-correlated cross-relaxation rates. **a)** Correlation plot between the calculated unscaled and scaled longitudinal CSA/DD cross-correlated cross-relaxation rates with the measured rates at 14.1 T and 18.8 T. The black line is shown as a guide for perfect equality between the two rates. **b)** Correction factors as a function of the magnetic field for Ile-30 and Ile-44 with or without scaling of the longitudinal CSA/DD cross-correlated cross-relaxation rate.

768 sured and corrected relaxometry relaxation rates at the same magnetic field
769 (Fig. 10a). The uncorrected relaxometry rates $R_1(^{13}\text{C})$ are systematically
770 lower than the accurate relaxation rates. This stresses the fact that the re-
771 laxometry relaxation rates have to be corrected in order to reach a reliable
772 analysis of the properties the dynamics of the system. Corrected rates are
773 in excellent agreement with the accurate $R_1(^{13}\text{C})$ rates measured with the
774 two-field system. This comparison validates the ICARUS approach on this
775 spin system. In addition, experiments have been recorded at 14.1 T with and
776 without pulses during the relaxation delay. Corresponding relaxation rates
777 are displayed in Fig. 10b. The high-field experiment recorded without control
778 of cross-relaxation pathways is similar to a shuttling experiments. Correction
779 factors seem to be slightly overestimated at 14.1 T, but corrected rates are
780 in better agreement with accurate rates than uncorrected rates (r.m.s.d of
781 $3.8 \times 10^{-2} \text{ s}^{-1}$ versus $5.7 \times 10^{-2} \text{ s}^{-1}$, respectively).

782 5. Conclusion

783 In this paper, we have presented a general framework for the analysis
784 of high-resolution relaxometry data. First, REDKITE is a powerful MATH-
785 EMATICA notebook to calculate relaxation rates and entire relaxation ma-
786 trices in any nuclear spin system. We have shown how it can be used for
787 the analysis of HRR, but it can also be applied more generally for the study
788 of relaxation properties. Second, ICARUS is a PYTHON-based program de-
789 signed to analyze relaxometry datasets accounting for the effects of multiple
790 cross-relaxation pathways. The two toolkits have been developed in order
791 to be easily adapted to other spin systems, diffusion tensors and models of
792 motions. Conclusions drawn here in the case of a $\{^{13}\text{C}^1\text{H}^2\text{H}_2\}$ -methyl group
793 with respect to the effect of the size of the relaxation matrix, the number
794 of iteration of ICARUS or the model for the spectral density function may
795 be different in other systems. Overall, a complete analysis by REDKITE and
796 ICARUS can be performed quickly, allowing one to evaluate these effects ef-
797 ficiently. Our approach to correct high-resolution relaxometry data has been
798 cross-validated by the measurements of accurate low-field relaxation rates.

799 6. Materials and methods

800 Methods to obtain carbon-13 and proton longitudinal relaxation rates at
801 0.33 T were previously described [21] and are based on the use of a two-field

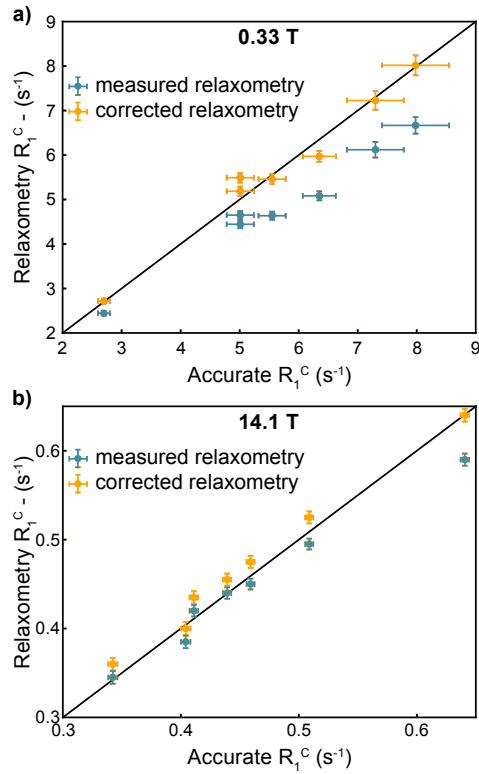


Figure 10: Validation of the correction protocol. **a)** Correlation plot between the relaxometry uncorrected (blue) and corrected (orange) carbon R_1 at 0.33 T with the measured two-field $R_1(^{13}C)$. **b)** Correlation plot between the pseudo-relaxometry uncorrected (blue) and corrected (orange) $R_1(^{13}C)$ with the accurate relaxation rates measured at 14.1 T. The black line is shown as a guide for perfect equality between the two rates.

802 spectrometer operating at 14.1 T and 0.33 T [20, 19]. Proton longitudinal
803 relaxation rates at 14.1 T and 18.8 T were measured following methods in-
804 troduced earlier [37]. Carbon-13 inversion pulses were applied during the
805 relaxation period every 40 ms and a proton inversion pulse was applied in
806 the middle of the relaxation delay. The experiment was performed with the
807 following relaxation delays: 0.08*, 0.24, 0.48, 0.72, 0.96, 1.28, 1.68, 2.08,
808 2.48, 2.88*, 3.28, 3.68, 4.08 s (the measurements marked by a star have been
809 performed twice).

810 The longitudinal and transverse cross-correlated cross-relaxation rates (η_z^C
811 and η_{xy}^C) were measured using the symmetrical reconversion principle [62, 40].
812 For enhanced sensitivity, cross-relaxation experiments were accumulated with
813 8-times more scans than auto-relaxation experiments. The longitudinal cross-
814 correlated cross-relaxation rate at 18.8 T was determined with a relaxation
815 delay of 1.5 s, while at 14.1 T the experiment was performed with the re-
816 laxation delays of 1.0, 1.5, and 2.0 s. The measurement of the transverse
817 cross-correlated cross relaxation rate was done using a spin lock irradiation
818 with amplitudes of 2031 and 2062 Hz at 14.1 and 18.8 T, respectively. The
819 alignment of the spins into the direction of the spin-lock field and back to
820 z-direction was achieved using adiabatic half passage pulses. The calibration
821 of the spin lock rf amplitude was done by measuring the scaling of scalar
822 couplings under off-resonance continuous wave irradiation. The transverse
823 cross-correlated cross relaxation rate at 18.8 T was determined from a single
824 experiment performed with the relaxation delay 250 ms, while the experiment
825 was repeated twice with the relaxation delays 175 and 250 ms at 14.1 T.
826 The measurement of the "relaxometry-like" relaxation rate at 14.1 T was
827 performed with the standard pulse program to measure longitudinal relax-
828 ation rates [37], but all pulses usually applied during the relaxation period
829 were omitted. The experiment was measured twice, first with the relaxation
830 delays 0.06*, 0.18, 0.38, 0.62, 0.94, 1.26*, 1.62, 2.02 s, and second with relax-
831 ation delays 0.61*, 0.73, 0.93, 1.17, 1.49, 1.81*, 2.17, 2.57 s (the star denotes
832 measurements repeated once).

833 **Data availability**

834 REDKITE can be found here: <https://figshare.com/articles/RedKite/11745111>
835 The ICARUS suite (ICARUS, MCMC script and RedKite2ICARUS) can be
836 found here: <https://figshare.com/articles/ICARUS/9893912>

837 **CRedit author statement**

838 **Nicolas Bolik-Coulon**: software, conceptualization, formal analysis,
839 data curation, writing - original draft, visualization **Pavel Kadeřávek**: data
840 curation, resources, investigation, validation **Philippe Pelupessy**: formal
841 analysis, validation **Jean-Nicolas Dumez**: conceptualization, formal analy-
842 sis, supervision, writing - review & editing, validation **Fabien Ferrage**: con-
843 ceptualization, formal analysis, funding acquisition, project administration,
844 supervision, writing - review & editing **Samuel F. Cousin**: software, con-
845 ceptualization, formal analysis, data curation, investigation, writing - original
846 draft, visualization.

847 **Acknowledgement**

848 This project received funding from the European Research Council (ERC)
849 under the European Union's Seventh Framework Programme (FP7/2007-
850 2013), ERC Grant agreement 279519 (2F4BIODYN).

851 **References**

- 852 [1] R. R. Ernst, W. A. Anderson, Rev. Sci. Instrumental. 37 (1966) 93.
- 853 [2] K. Pervushin, R. Riek, G. Wider, K. Wuthrich,
854 Proc. Natl. Acad. Sci. USA 94 (1997) 12366.
- 855 [3] V. Tugarinov, P. M. Hwang, J. E. Ollerenshaw, L. E. Kay,
856 J. Am. Chem. Soc. 125 (2003) 10420.
- 857 [4] H. Shimizu, J. Chem. Phys. 40 (1964) 3357.
- 858 [5] M. Goldman, J. Magn. Reson. 60 (1984) 437.
- 859 [6] S. Wimperis, G. Bodenhausen, Molec. Phys. 66 (1989) 897.
- 860 [7] L. G. Werbelow, A. G. Marshall, J. Magn. Reson. 11 (1973) 299.
- 861 [8] M. Carravetta, O. G. Johannessen, M. H. Levitt, Phys. Rev. Lett. 92
862 (2004) 153003.
- 863 [9] M. Carravetta, M. H. Levitt, J. Chem. Phys. 122 (2005) 214505.

- 864 [10] J. H. Ardenkjaer-Larsen, B. Fridlund, A. Gram, G. Hansson,
865 L. Hansson, M. H. Lerche, R. Servin, M. Thaning, K. Golman,
866 Proc. Natl. Accad. Sci. USA 100 (2003) 10158.
- 867 [11] J. Milani, B. Vuichoud, A. Bornet, P. Miéville, R. Mottier, S. Jannin,
868 G. Bodenhausen, Rev. Sci. Instrum. 86 (2015) 024101.
- 869 [12] S. Bowen, C. Hilty, Angew. Chem. Int. Ed. 47 (2008) 5235.
- 870 [13] R. Kimmich, E. Anorado, Prog. Nucl. Magn. Reson. Spectrosc. 44 (2004)
871 257.
- 872 [14] A. G. Redfield, Magn. Reson. Chem. 41 (2003) 753.
- 873 [15] A. G. Redfield, J. Biomol. NMR. 52 (2012) 159.
- 874 [16] C.-Y. Chou, M. Chu, C.-F. Chang, T.-h. Huang, J. Magn. Reson. 214
875 (2012) 302.
- 876 [17] C. Charlier, S. N. Khan, T. Marquardsen, P. Pelupessy, V. Reiss,
877 D. Sakellariou, G. Bodenhausen, F. Engelke, F. Ferrage,
878 J. Am. Chem. Soc. 135 (2013) 18665.
- 879 [18] S. Korchak, K. Ivanov, A. Yurkovskaya, H.-M. Vieth, J. Chem. Phys.
880 133 (2010) 194502.
- 881 [19] S. F. Cousin, C. Charlier, P. Kadeřávek, T. Marquardsen, J.-M. Ty-
882 burn, P.-A. Bovier, S. Ulzega, T. Speck, D. Wilhelm, F. Engelke,
883 W. Maas, D. Sakellariou, G. Bodenhausen, P. Pelupessy, F. Ferrage,
884 Phys. Chem. Chem. Phys. 18 (2016) 33187.
- 885 [20] S. S. F. Cousin, P. Kadeřávek, B. Haddou, C. Charlier, T. Marquardsen,
886 J.-M. J.-M. Tyburn, P.-A. P.-A. Bovier, F. Engelke, W. Maas, G. Bo-
887 denhausen, P. Pelupessy, F. Ferrage, Angew. Chem. Int. Ed. 55 (2016)
888 9886.
- 889 [21] P. Kadeřávek, N. Bolik-Coulon, S. F. Cousin, T. Marquardsen, J.-M.
890 Tyburn, J.-N. Dumez, F. Ferrage, J. Phys. Chem. Lett. 10 (2019) 5917.
- 891 [22] M. H. Levitt, L. Di Bari, Bulletin of Magnetic Resonance 16 (1994) 94.
- 892 [23] M. F. Roberts, A. G. Redfield, J. Am. Chem. Soc 126 (2004) 13765.

- 893 [24] M. W. Clarkson, M. Lei, E. Z. Eisenmesser, W. Labeikovsky, A. Redfield,
894 D. Kern, *J. Biomol. NMR.* 45 (2009) 217.
- 895 [25] S. F. Cousin, P. Kadeřávek, N. Bolik-Coulon, Y. Gu, C. Char-
896 lier, L. Carlier, L. Bruschiweiler-Li, T. Marquardsen, J.-M. Tyburn,
897 R. Brüschiweiler, F. Ferrage, *J. Am. Chem. Soc.* 140 (2018) 13456.
- 898 [26] S. F. Cousin, P. Kadeřávek, N. Bolik-Coulon, F. Ferrage, Determination
899 of protein ps-ns motions by high-resolution relaxometry, in: *Methods in*
900 *Molecular Biology*, Vol. 1688, Springer, 2018, p. 169.
- 901 [27] A. Jerschow, *J. Magn. Reson.* 176 (2005) 7.
- 902 [28] I. Kuprov, N. Wagner-Rundell, P. Hore, *J. Magn. Reson.* 184 (2007) 196.
- 903 [29] C. Bengs, M. H. Levitt, *Magn. Reson. Chem.* 56 (2018) 374.
- 904 [30] I. Wolfram Research, *Mathematica* (2016).
- 905 [31] A. Kumar, C. R. R. Grace, P. K. Madhu,
906 *Prog. Nucl. Magn. Reson. Spectrosc.* 37 (2000) 191.
- 907 [32] J. Kowalewski, L. Mäler, *Nuclear Spin Relaxation in Liquids: Theory,*
908 *Experiments, and Applications*, Taylor & Francis, 2006.
- 909 [33] M. P. Nicholas, E. Eryilmaz, F. Ferrage, D. Cowburn, R. Ghose,
910 *Prog. Nucl. Magn. Reson. Spectrosc.* 57 (2010) 111.
- 911 [34] A. Abragam, *The Principles of Nuclear Magnetism*, Oxford University
912 Press, London, 1961.
- 913 [35] J. Kowalewski, L. Werbelow, *J. Magn. Reson.* 128 (1997) 144.
- 914 [36] R. Paquin, P. Pelupessy, L. Duma, C. Gervais, G. Bodenhausen,
915 *J. Chem. Phys.* 133 (2010) 034506.
- 916 [37] F. Ferrage, *Methods Mol. Biol.* 831 (2012) 141.
- 917 [38] M. H. Levitt, L. D. Bari, *Bull. Magn Reson.* 16 (1994) 94.
- 918 [39] R. Ghose, *Concepts Magn. Reson.* 12 (2000) 152.

- 919 [40] P. Pelupessy, F. Ferrage, G. Bodenhausen, *J. Chem. Phys.* 126 (2007)
920 134.
- 921 [41] N. Bolik-Coulon, S. F. Cousin, P. Kadeřávek, J.-N. Dumez, F. Ferrage,
922 *J. Chem. Phys.* 150 (2019) 224202.
- 923 [42] J. Cavanagh, W. J. Fairbrother, A. G. Palmer, M. Rance, N. J. Skelton,
924 *Protein NMR Spectroscopy: Principles and Practice*, Elsevier Academic
925 Press, 2007.
- 926 [43] G. Lipari, A. Szabo, *J. Am. Chem. Soc.* 104 (1982) 4546.
- 927 [44] M. Novakovic, S. F. Cousin, M. J. Jaroszewicz, R. Rosenzweig, L. Fry-
928 dman, *J. Magn. Reson.* 294 (2018) 169.
- 929 [45] D. J. Wales, J. P. K. Doye, *J. Phys. Chem. A* 101 (1997) 5111.
- 930 [46] D. Foreman-Mackey, D. W. Hogg, D. Lang, J. Goodman,
931 *Publ. Astron. Soc. Pac.* 125 (2013) 306.
- 932 [47] V. Tugarinov, V. Kanelis, L. E. Kay, *Nat. Protoc.* 1 (2006) 749.
- 933 [48] M. J. Plevin, J. Boisbouvier, *Isotope-Labeling of Methyl Groups for*
934 *NMR Studies of Large Proteins*, Royal Society of Chemistry, 2012, Ch. 1,
935 pp. 1–24.
- 936 [49] G. Mas, E. Crublet, O. Hamelin, P. Gans, J. Boisbouvier,
937 *J. Biomol. NMR* 57 (2013) 251.
- 938 [50] K. H. DuBay, G. R. Bowman, P. L. Geissler, *Acc. Chem. Res.* 48 (2015)
939 1098.
- 940 [51] K. K. Frederick, M. S. Marlow, K. G. Valentine, J. Wand, *Nature* 448
941 (2007) 325.
- 942 [52] G. M. Clore, A. Szabo, A. Bax, L. E. Kay, P. C. Driscoll, A. M. Gro-
943 nenborn, *J. Am. Chem. Soc.* 112 (1990) 4989.
- 944 [53] E. Meirovitch, Y. E. Shapiro, A. Polimeno, J. H. Freed, *J. Phys. Chem. A*
945 110 (2006) 8366.
- 946 [54] E. Meirovitch, Y. E. Shapiro, A. Polimeno, J. H. Freed, *J. Phys. Chem. B*
947 111 (2007) 12865.

- 948 [55] C. Charlier, S. F. Cousin, F. Ferrage, *Chem. Soc. Rev.* 45 (2016) 2410.
- 949 [56] V. Calandrini, D. Abergel, G. R. Kneller, *J. Chem. Phys.* 133 (2010)
950 145101.
- 951 [57] S. N. Khan, C. Charlier, R. Augustyniak, N. Salvi, V. Déjean, G. Bo-
952 denhausen, O. Lequin, P. Pelupessy, F. Ferrage, *Biophys. J.* 109 (2015)
953 988.
- 954 [58] A. Hsu, F. Ferrage, A. G. Palmer, *Biophys. J.* 115 (2018) 2301.
- 955 [59] D. Frueh, *Prog. Nucl. Magn. Reson. Spectrosc.* 41 (2002) 305.
- 956 [60] L. G. Werbelow, D. M. Grant, *J. Chem. Phys.* 63 (1975) 544.
- 957 [61] V. Tugarinov, C. Scheurer, R. Brüschweiler, L. E. Kay, *J. Biomol. NMR*
958 30 (2004) 397.
- 959 [62] P. Pelupessy, G. M. Espallargas, G. Bodenhausen, *J. Magn. Res.* 161
960 (2003) 258.
- 961 [63] N. Tjandra, S. E. Feller, R. W. Pastor, A. Bax, *J. Am. Chem. Soc.* 117
962 (1995) 12562.
- 963 [64] A. Mittermaier, L. E. Kay, *J. Am. Chem. Soc.* 121 (1999) 10608.

965 **Contents**

966	1	Size-reduction of relaxation matrices by removing fast-relaxing operators	49
967			
968	2	Correlation functions and spectral density functions	50
969	3	Set up of REDKITE for the $\{^{13}\text{C}^1\text{H}^2\text{H}_2\}$-methyl groups of Ubiquitin with a vicinal deuterium	52
970			
971	3.1	Definition of the spin system	52
972	3.2	Spectral density function	54
973	3.3	Relaxation matrix	54
974	3.4	Relaxation rates	55
975	3.5	Export	55
976	3.6	Conversion to a FunctionsFile	55
977	4	Expression of the relaxation matrix in the reduced basis	56
978	4.1	Relaxation matrix	56
979	4.2	Auto-relaxation rates	58
980	4.3	Cross-relaxation rates	61
981	5	Figures	63
982	6	Hamiltonian in REDKITE	64
983	7	Tables	66

984 **1. Size-reduction of relaxation matrices by removing fast-relaxing**
 985 **operators**

986 Here, we will show that fast-relaxing terms of a relaxation matrix can be
 987 discarded (as done in Section 4.2.5 of the main text) in order to reduce the
 988 size of the relaxation matrix and save computational time. For the sake of
 989 simplicity, we consider a 2x2 Liouvillian:

$$\mathcal{L} = \begin{pmatrix} R_1 & \sigma \\ \sigma & R'_1 \end{pmatrix}. \quad (44)$$

990 The characteristic polynomial of \mathcal{L} is:

$$\det[\mathcal{L} - \lambda\mathcal{I}] = \lambda^2 - \lambda(R_1 + R'_1) - \sigma^2 + R_1R'_1, \quad (45)$$

991 with \mathcal{I} the identity matrix. The roots are given by:

$$\lambda_{\pm} = \frac{R_1 + R'_1 \pm \sqrt{\Delta}}{2}, \quad (46)$$

992 with:

$$\Delta = R_1'^2 + R_1^2 - 2R_1R'_1 + 4\sigma^2. \quad (47)$$

993 Let's assume $R'_1 \gg R_1, \sigma$. A first order approximation in R_1 and σ of $\sqrt{\Delta}$
 994 leads to:

$$\sqrt{\Delta} \approx R'_1 \left(1 - \frac{R_1}{R'_1}\right) = R'_1 - R_1, \quad (48)$$

995 such that the eigenvalues of \mathcal{L} are R_1 and R'_1 . The associated eigenvectors
 996 approximate to $\{1, 0\}$ and $\{0, 1\}$ and the autorelaxation of the operator of
 997 interest can be considered mono-exponential with decay rate of R_1 . The fast
 998 relaxing operator does not contribute to the relaxation of the slowly relaxing
 999 operator.

1000 This can be verified by simulating the polarization decay. We will set $R_1 =$
 1001 1 s^{-1} , $\sigma = 0.5 \text{ s}^{-1}$ and vary R'_1 . We can compute the polarization decay (as-
 1002 sociated with the operator of interest with autorelaxation rate R_1) following
 1003 Section 2.2 of the main text (Fig. S1). The polarization decay can be fitted
 1004 to a mono-exponential decay, and fitted relaxation rates are reported in Ta-
 1005 ble S1. It is clear that the fast relaxing operator has negligible effects on
 1006 the polarization decay when $R'_1 \gg R_1$.

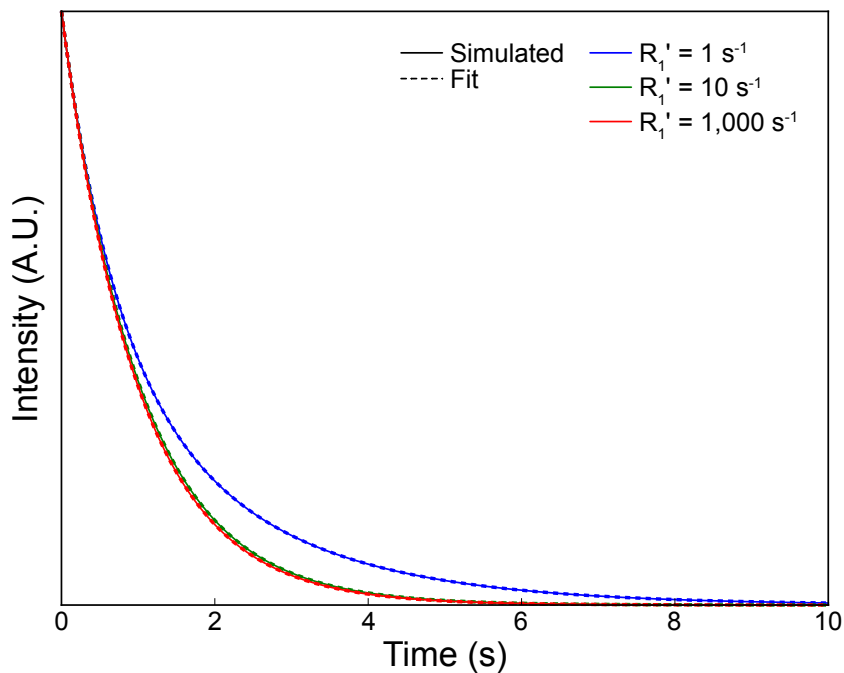


Figure S1: Simulated polarization decay (plain) and exponential fit (dash) for different values of R_1' relaxation rates.

Table S1: Fitted relaxation rates from the simulated polarization decay for different values of R_1'

R_1' (s^{-1})	fitted relaxation rate (s^{-1})
1	0.73
10	0.97
1,000	1.00

1007 2. Correlation functions and spectral density functions

1008 The choice of the model of motions is a key step in the analysis of relax-
 1009 ation rates to characterize quantitatively protein dynamics. The description
 1010 of models of correlation functions can be found elsewhere [43, 52, 53, 54, 55,
 1011 56, 57]. Any analytical form of the spectral density function can be used in

1012 REDKITE and ICARUS. Assuming that different types of motions are statis-
 1013 tically independent, the overall correlation function $\mathcal{C}_{i,j}$ associated to auto- or
 1014 cross-correlation of interaction(s) (i, j) can be written as the product of the
 1015 correlation function of overall rotation \mathcal{C}_g , assumed here to be isotropic, and
 1016 of the individual motions $\mathcal{C}_{i,j}^n$, all supposed to be independent and isotropic:

$$\mathcal{C}_{i,j}(t) = \mathcal{C}_g(t) \prod_n \mathcal{C}_{i,j}^n(t). \quad (49)$$

1017 In model-free approaches, the overall rotation correlation function $\mathcal{C}_{i,j}$ is de-
 1018 scribed by a single exponential decay for isotropic diffusion, or a sum of
 1019 exponentials for axially symmetric or fully anisotropic rotational diffusion
 1020 [63]. The correlation function used for the model-free $\mathcal{C}_{i,j}^{\text{MF}}$ and extended
 1021 model-free $\mathcal{C}_{i,j}^{\text{EMF}}$ approaches are:

$$\begin{aligned} \mathcal{C}_{i,j}^{\text{MF}}(t) &= e^{-t/\tau_g} \left(S^2 + (\mathcal{P}_2(\cos \theta_{i,j}) - S^2) e^{-t/\tau_{\text{int}}} \right), \\ \mathcal{C}_{i,j}^{\text{EMF}}(t) &= e^{-t/\tau_g} \left(S_f^2 S_s^2 + (\mathcal{P}_2(\cos \theta_{i,j}) - S_f^2) e^{-t/\tau_f} \right. \\ &\quad \left. + S_f^2 (\mathcal{P}_2(\cos \theta_{i,j}) - S_s^2) e^{-t/\tau_s} \right), \end{aligned} \quad (50)$$

1022 where $\theta_{i,j}$ is the angle between the principal axes of the two interactions,
 1023 $\mathcal{P}_2(x)$ is the second order Legendre polynomial $\mathcal{P}_2(x) = (3x^2 - 1)/2$, τ_g the
 1024 correlation time for the global tumbling. The correlation function for the
 1025 model-free approach is defined by the effective correlation time τ_{int} and the
 1026 order parameter S^2 . In the extended model-free correlation function, τ_s (re-
 1027 spectively τ_f) is the correlation time associated with the order parameter S_s^2
 1028 (respectively S_f^2) for the slower (respectively faster) motion. The correspond-
 1029 ing spectral density functions $\mathcal{J}_{i,j}^{\text{MF}}(\omega)$ and $\mathcal{J}_{i,j}^{\text{EMF}}(\omega)$ can be used for both
 1030 auto- and cross-correlation of interactions:

$$\begin{aligned} \mathcal{J}_{i,j}^{\text{MF}}(\omega) &= \frac{1}{5} \left(\frac{S^2 \tau_g}{1 + (\omega \tau_g)^2} + \frac{(\mathcal{P}_2(\cos \theta_{i,j}) - S^2) \tau'}{1 + (\omega \tau')^2} \right), \\ \mathcal{J}_{i,j}^{\text{EMF}}(\omega) &= \frac{1}{5} \left(\frac{S_f^2 S_s^2 \tau_g}{1 + (\omega \tau_g)^2} + \frac{(\mathcal{P}_2(\cos \theta_{i,j}) - S_f^2) \tau'_f}{1 + (\omega \tau'_f)^2} + \frac{S_f^2 (1 - S_s^2) \tau'_s}{1 + (\omega \tau'_s)^2} \right), \end{aligned} \quad (51)$$

1031 where τ'_a is the effective correlation time defined as $\tau'_a{}^{-1} = \tau_a^{-1} + \tau_g^{-1}$.
 1032 Other correlation functions can be used depending on the system under study.
 1033 For example, the correlation function can be written as a sum of exponential
 1034 functions:

$$\mathcal{C}_{\Sigma \text{ exp}}(t) = \sum_{i=1}^n A_i e^{-t/\tau_i}. \quad (52)$$

1035 The corresponding spectral density is:

$$\mathcal{J}_{\Sigma \text{ exp}}(t) = \frac{1}{5} \sum_{i=1}^n A_i \frac{\tau_i}{1 + (\omega\tau_i)^2}. \quad (53)$$

1036 In the case of relaxation in a methyl group, assuming the statistical inde-
 1037 pendence of the methyl group rotation, the motions of the methyl group
 1038 axis and the overall rotational diffusion, the correlation function $C_{i,j}^{\text{met}}$ can
 1039 be expressed as the product of the three corresponding correlation functions:
 1040 C_g for the global tumbling, $C_{\text{rot}}^{i,j}$ for the methyl group rotation, C_{axis} for the
 1041 complex motions of the methyl group. The correlation function was given in
 1042 the main text (Eq. 36). The rotation of the methyl group is an anisotropic
 1043 motion characterized by the correlation time τ_{met} and the order parameter
 1044 $S_{\text{met}}^2(\theta_{i,j})$ imposed by the geometry of the methyl group (supposed to be a
 1045 tetrahedron, three corners of which are occupied by the proton and the two
 1046 deuterium nuclei and the center by the carbon-13) and the relative orienta-
 1047 tions of the principal axes of interactions i and j with respect to the methyl
 1048 axis. Motions of the methyl group axis are described by an extended model-
 1049 free correlation function, with the parameters S_f^2 , τ_f , S_s^2 , and τ_s , as is detailed
 1050 in the main text.

1051 **3. Set up of REDKITE for the $\{^{13}\text{C}^1\text{H}^2\text{H}_2\}$ -methyl groups of Ubiquitin with a vicinal deuterium**

1052

1053 Here, we show the most important command lines used to calculate re-
 1054 laxation rates and relaxation matrix of a $\{^{13}\text{C}^1\text{H}^2\text{H}_2\}$ -methyl group with a
 1055 vicinal deuterium nucleus.

1056 *3.1. Definition of the spin system*

1057 Nuclei = {{"13C", "CA"}, {"1H", "HA"}, {"2H", "DA"}, {"2H", "DB"},
 1058 {"2H", "DC"}};

The deuterium DC is associated with the vicinal deuterium here. The *SetSpinSystem* command is then run as explained in the main text without any

changes. We define the intermediate constants:

$$\begin{aligned}
\alpha &= 109.47\pi/180; \\
\text{aCH} &= \pi - \alpha; \\
\text{rCH} &= 1.115 \times 10^{-10}; \\
\text{rCD} &= 1.115 \times 10^{-10}; \\
\text{hCH} &= \text{rCH} \times \text{Cos}[\text{aCH}]; \\
\text{hCD} &= \text{rCD} \times \text{Cos}[\text{aCH}]; \\
\text{OH} &= \text{Sqrt}[\text{rCD}^2 - \text{hCH}^2]; \\
\text{OD} &= \text{Sqrt}[\text{rCD}^2 - \text{hCD}^2]; \\
\text{ryCD} &:= \text{rxyCDvic}; \\
\text{rzCD} &:= \text{rzCDvic};
\end{aligned}$$

before definition of the atoms coordinates:

$$\begin{aligned}
\text{Coordinates} &= \{ \{0, 0, 0\}, \\
&\quad \{0, -\text{OH}, \text{hCH}\}, \\
&\quad \{(\text{Sqrt}[3]/2)\text{OD}, 2\text{OD}/2, \text{hCD}\}, \\
&\quad \{-(\text{Sqrt}[3]/2)\text{OD}, 2\text{OD}/2, \text{hCD}\}, \\
&\quad \{0, \text{ryCD}, \text{rzCD}\};
\end{aligned}$$

The carbon-13 is set at the origin of the Cartesian axis system, the ^1H is in the Oyz plan, as is the vicinal deuterium, which position is determined by two unknown (later optimized) variables describing its position along axes Oy and Oz (ryCD and rzCD , respectively). The two deuterium nuclei of the methyl group are mirror image of one another with respect to the Oyz plane. We define a System Frame with z-axis along the symmetry axis of the methyl group, *i.e.* the Oz axis:

$$\text{SF} = \{0, 0, 1\};$$

The orientation of the interactions relative to the System Frame is important when studying the dynamics of the methyl groups, in particular their rotation around the symmetry axis, and are used in the definition of the spectral density function (see main text).

We only consider the CSA for the carbon-13 nucleus, assumed to be axially symmetric:

$$\text{CSAConsidered} = \{1, 0, 0, 0, 0\};$$

with value CSAValue which will be a variable optimized during the analysis of relaxation data:

$$\delta_{csa}[1] = CSAValue;$$

1059 and oriented along the CC bond (*i.e.* the symmetry axis):

1060
$$\text{vectorNum}_1^{\text{CSA}} = \{0, 0, 1\};$$

Finally, we consider the quadrupolar interaction of the methyl deuterium nuclei, but not for the vicinal deuterium [64]:

$$\begin{aligned} d_Q[1] &= 0; \\ d_Q[2] &= 0; \\ d_Q[3] &= 167000 * 2 * \pi; \\ d_Q[4] &= 167000 * 2 * \pi; \\ d_Q[5] &= 0; \end{aligned}$$

1061 and we define the orientations of the considered quadrupolar interactions:

1062
$$\begin{aligned} \text{vectorNum}_3^{\text{Quad}} &= \text{Vec}["CA", "DA"]; \\ \text{vectorNum}_4^{\text{Quad}} &= \text{Vec}["CA", "DB"]; \\ \text{vectorNum}_5^{\text{Quad}} &= \{0, 0, 0\}; \end{aligned}$$

1063 where the command *Vec* extracts the vector between the two entries (the
1064 two nuclei). In the following analytical expressions of relaxation rates, the
1065 intensity of the quadrupolar interaction will be labelled ζ_Q .

1066 3.2. Spectral density function

1067 We used the same spectral density function written in Eq. 37 of the main
1068 text. We assumed the vicinal deuterium nucleus follows the same model of
1069 spectral density function, even if it is not sensitive to the rotation of the
1070 methyl group as the ^{13}C , ^1H and deuterium nuclei are. Note that the two
1071 parameters used to position the effective vicinal deuterium nucleus change
1072 the effect of the methyl group rotation on relative correlation functions.

1073 3.3. Relaxation matrix

1074 The longitudinal relaxation rates measured during the relaxometry ex-
1075 periment correspond to the operator \hat{C}_z . Thus:

1076
$$\text{OperatorOfInterest} = \text{opI}["CA", "z"];$$

1077 The basis contains 11,664 terms, and is first reduced to 24 terms, as detailed
 1078 in the main text. Calculations shows that the decays of the \hat{C}_z longitudi-
 1079 nal polarization is well described using the subspace $\left\{ \frac{\hat{C}_z}{3\sqrt{3}}, \frac{\hat{H}_z}{3\sqrt{3}}, \frac{2\hat{C}_z\hat{H}_z}{3\sqrt{3}} \right\}$, as
 1080 detailed in the main text. The relaxation matrix is computed using this
 1081 basis.

1082 3.4. Relaxation rates

1083 During the course of the analysis of U-[^2H , ^{15}N], Ile- δ_1 [$^{13}\text{C}^2\text{H}_2^1\text{H}$]-Ubiquitin dy-
 1084 namics, ^{13}C and ^1H longitudinal relaxation rates, ^{13}C transverse relaxation
 1085 rate and ^{13}C - ^1H cross-relaxation rates were measured. This leads to:

```

1086 RatesOfInterest = {
    {Rate[opI["HA", "z"], opI["HA", "z"]], "R1H"},
    {Rate[opI["CA", "z"], opI["HA", "z"]], "R1C"},
    {Rate[opI["CA", "+"], opI["CA", "+" ]], "R2C"},
    {Rate[opI["CA", "z"], opI["HA", "z"]], "Sigma"}
  }

```

1087 3.5. Export

1088 Export has to be done carefully as the introduction of numerically un-
 1089 known positions for the vicinal deuterium introduces complications when
 1090 automatically detecting the variables of the system (important in order to
 1091 calculate the derivatives). This has to be corrected manually within RED-
 1092 KITE.

1093 3.6. Conversion to a FunctionsFile

1094 When defining the ^{13}C -CSA, it was chosen to keep it as a variable that
 1095 would be further optimized during the analysis of the relaxometry relaxation
 1096 rates.

1097 **4. Expression of the relaxation matrix in the reduced basis**

1098 *4.1. Relaxation matrix*

1099 Operators in the secularized basis are:

$$\mathcal{B}_{\text{secularized}} = \left\{ \frac{\hat{C}_z}{3\sqrt{3}}, \frac{\hat{H}_z}{3\sqrt{3}}, \frac{2\hat{C}_z\hat{H}_z}{3\sqrt{3}}, \frac{\sqrt{2}\hat{C}_z\hat{H}_z\hat{D}_{1,z}}{3}, \frac{\sqrt{2}\hat{C}_z\hat{H}_z\hat{D}_{2,z}}{3}, \frac{\hat{C}_z\hat{D}_{1,z}}{3\sqrt{3}}, \frac{\hat{C}_z\hat{D}_{2,z}}{3\sqrt{3}}, \right. \\ \left. \frac{\hat{D}_{1,z}}{6\sqrt{2}}, \frac{\hat{D}_{2,z}}{6\sqrt{2}}, \frac{\hat{C}_z\hat{D}_1^-\hat{D}_2^+}{4\sqrt{3}}, \frac{\hat{C}_z\hat{D}_1^+\hat{D}_2^-}{4\sqrt{3}}, \frac{\hat{C}_z\hat{D}_{1,z}\hat{D}_{2,z}}{2\sqrt{3}}, \frac{3\hat{C}_z\hat{D}_{1,z}\hat{D}_{1,z} - 2\hat{C}_z}{3\sqrt{6}}, \right. \\ \left. \frac{3\hat{C}_z\hat{D}_{2,z}\hat{D}_{2,z} - 2\hat{C}_z}{3\sqrt{6}} \right\}. \quad (54)$$

Note that numerical simulations were carried out in a reduced basis formed with elements $\frac{\hat{C}_z}{3\sqrt{3}}$, $\frac{\hat{H}_z}{3\sqrt{3}}$ and $\frac{2\hat{C}_z\hat{H}_z}{3\sqrt{3}}$ of the secularized basis. The relaxation

matrix is:

$$\begin{bmatrix} R_1(^{13}\text{C}) & \sigma_{\text{CH}} & \eta_z^{\text{C}} & \kappa^{\text{C}} & \kappa^{\text{C}} & \eta_z^{\text{CD}} & \eta_z^{\text{CD}} & \eta_z^{\text{CD}} & \sigma_{\text{CD}} & \lambda & \lambda & \nu_z & \mu & \mu \\ \sigma_{\text{CH}} & R_1(^1\text{H}) & 0 & \kappa^{\text{H}} & \kappa^{\text{H}} & 0 & 0 & 0 & \sigma_{\text{HD}} & 0 & 0 & 0 & 0 & 0 \\ \eta_z^{\text{C}} & 0 & R_{\text{CH}} & \kappa^{\text{CH}} & \kappa^{\text{CH}} & \delta & \delta & \delta & \sigma_{\text{HD}} & 0 & 0 & 0 & 0 & 0 \\ \kappa^{\text{C}} & \kappa^{\text{H}} & \kappa^{\text{CH}} & R_{\text{CHD}} & R_{\text{CHD}} & \eta_z^{\text{CHD}} & \eta_z^{\text{CHD}} & \eta_z^{\text{CHD}} & \sigma_{\text{CHD}} & \lambda^{(1)} & \lambda^{(1)} & \nu_z^{(1)} & \mu^{(1)} & 0 \\ \kappa^{\text{C}} & \kappa^{\text{H}} & \kappa^{\text{CH}} & \kappa^{\text{CHD}} & R_{\text{CHD}} & 0 & 0 & 0 & \sigma_{\text{CHD}} & \lambda^{(1)} & \lambda^{(1)} & \nu_z^{(1)} & 0 & \mu^{(1)} \\ \eta_z^{\text{CD}} & 0 & \delta & \eta_z^{\text{CHD}} & \eta_z^{\text{CHD}} & 0 & R_{\text{CD}} & R_{\text{CD}} & 0 & 0 & 0 & \nu_z^{(2)} & \mu^{(2)} & 0 \\ \eta_z^{\text{CD}} & 0 & \delta & 0 & \eta_z^{\text{CHD}} & 0 & \kappa^{\text{CD}} & R_{\text{CD}} & 0 & 0 & 0 & \nu_z^{(2)} & 0 & \mu^{(2)} \\ \sigma_{\text{CD}} & \sigma_{\text{HD}} & 0 & \sigma_{\text{CHD}} & \sigma_{\text{CHD}} & R_{\text{D}} & 0 & 0 & \sigma_{\text{DD}} & \lambda^{(2)} & \lambda^{(2)} & \nu_z^{(3)} & \mu^{(3)} & 0 \\ \sigma_{\text{CD}} & \sigma_{\text{HD}} & 0 & 0 & \sigma_{\text{CHD}} & R_{\text{D}} & 0 & 0 & R_{\text{D}} & \lambda^{(2)} & \lambda^{(2)} & \nu_z^{(3)} & 0 & \mu^{(3)} \\ \lambda & 0 & 0 & \lambda^{(1)} & \lambda^{(1)} & 0 & 0 & 0 & \lambda^{(2)} & \lambda^{(2)} & \kappa^{\text{CDD}} & \nu_z^{(4)} & \mu^{(4)} & \mu^{(4)} \\ \lambda & 0 & 0 & \lambda^{(1)} & \lambda^{(1)} & 0 & 0 & 0 & \lambda^{(2)} & \lambda^{(2)} & \kappa^{\text{CDD}} & \nu_z^{(4)} & \mu^{(4)} & \mu^{(4)} \\ \nu_z & 0 & 0 & \nu_z^{(1)} & \nu_z^{(1)} & \nu_z^{(2)} & \nu_z^{(2)} & \nu_z^{(2)} & \nu_z^{(3)} & R_{\text{CDD}}^{(1)} & R_{\text{CDD}}^{(1)} & R_{\text{CDD}}^{(2)} & \mu^{(5)} & \mu^{(5)} \\ \mu & 0 & 0 & \mu^{(1)} & \mu^{(1)} & 0 & 0 & 0 & 0 & \nu_z^{(4)} & \nu_z^{(4)} & \mu^{(5)} & R & 0 \\ \mu & 0 & 0 & \mu^{(1)} & \mu^{(1)} & 0 & 0 & 0 & \mu^{(3)} & \mu^{(4)} & \mu^{(4)} & \mu^{(5)} & 0 & R \end{bmatrix}$$

$$\begin{aligned}
R_1(^{13}\text{C}) &= \frac{2}{3}\Delta\sigma_C^2\omega_C^2\mathcal{J}_C(\omega_C) \\
&+ \frac{1}{2}d_{\text{CH}}^2(\mathcal{J}_{\text{CH}}(\omega_C - \omega_{\text{H}}) + 3\mathcal{J}_{\text{CH}}(\omega_C) + 6\mathcal{J}_{\text{CH}}(\omega_C + \omega_{\text{H}})) \\
&+ \frac{8}{3}d_{\text{CD}}^2(\mathcal{J}_{\text{CD}}(\omega_C - \omega_{\text{D}}) + 3\mathcal{J}_{\text{CD}}(\omega_C) + 6\mathcal{J}_{\text{CD}}(\omega_C + \omega_{\text{D}})) \\
&+ \frac{4}{3}d_{\text{CDvic}}^2(\mathcal{J}_{\text{CDvic}}(\omega_C - \omega_{\text{D}}) + 3\mathcal{J}_{\text{CDvic}}(\omega_C) + 6\mathcal{J}_{\text{CDvic}}(\omega_C + \omega_{\text{D}})), \\
R_1(^1\text{H}) &= \frac{1}{2}d_{\text{CH}}^2(\mathcal{J}_{\text{CH}}(\omega_C - \omega_{\text{H}}) + 3\mathcal{J}_{\text{CH}}(\omega_{\text{H}}) + 6\mathcal{J}_{\text{CH}}(\omega_C + \omega_{\text{H}})) \\
&+ \frac{8}{3}d_{\text{HD}}^2(\mathcal{J}_{\text{HD}}(\omega_{\text{D}} - \omega_{\text{H}}) + 3\mathcal{J}_{\text{HD}}(\omega_{\text{H}}) + 6\mathcal{J}_{\text{HD}}(\omega_{\text{D}} + \omega_{\text{H}})) \\
&+ \frac{4}{3}d_{\text{HDvic}}^2(\mathcal{J}_{\text{HDvic}}(\omega_{\text{D}} - \omega_{\text{H}}) + 3\mathcal{J}_{\text{HDvic}}(\omega_{\text{H}}) + 6\mathcal{J}_{\text{HDvic}}(\omega_{\text{D}} + \omega_{\text{H}})), \\
R_{\text{CH}} &= \frac{2}{3}\Delta\sigma_C^2\omega_C^2\mathcal{J}_C(\omega_C) + \frac{3}{2}d_{\text{CH}}^2(\mathcal{J}_{\text{CH}}(\omega_C) + \mathcal{J}_{\text{CH}}(\omega_{\text{H}})) \\
&+ \frac{8}{3}d_{\text{CD}}^2(\mathcal{J}_{\text{CD}}(\omega_C - \omega_{\text{D}}) + 3\mathcal{J}_{\text{CD}}(\omega_C) + 6\mathcal{J}_{\text{CD}}(\omega_C + \omega_{\text{D}})) \\
&+ \frac{8}{3}d_{\text{HD}}^2(\mathcal{J}_{\text{HD}}(\omega_{\text{H}} - \omega_{\text{D}}) + 3\mathcal{J}_{\text{HD}}(\omega_{\text{H}}) + 6\mathcal{J}_{\text{HD}}(\omega_{\text{H}} + \omega_{\text{D}})) \\
&+ \frac{4}{3}d_{\text{CDvic}}^2(\mathcal{J}_{\text{CDvic}}(\omega_C - \omega_{\text{D}}) + 3\mathcal{J}_{\text{CDvic}}(\omega_C) + 6\mathcal{J}_{\text{CDvic}}(\omega_C + \omega_{\text{D}})) \\
&+ \frac{4}{3}d_{\text{HDvic}}^2(\mathcal{J}_{\text{HDvic}}(\omega_{\text{H}} - \omega_{\text{D}}) + 3\mathcal{J}_{\text{HDvic}}(\omega_{\text{H}}) + 6\mathcal{J}_{\text{HDvic}}(\omega_{\text{H}} + \omega_{\text{D}})), \\
R_{\text{CHD}} &= \frac{3}{8}\zeta_{\text{Q}}^2(\mathcal{J}_{\text{Q}}(\omega_{\text{D}}) + 8\mathcal{J}_{\text{Q}}(2\omega_{\text{D}})) + \frac{2}{3}\Delta\sigma_C^2\omega_C^2\mathcal{J}_C(\omega_C) \\
&+ \frac{4}{3}d_{\text{DD}}^2(\mathcal{J}_{\text{DD}}(0) + 3\mathcal{J}_{\text{DD}}(\omega_{\text{D}}) + 6\mathcal{J}_{\text{DD}}(2\omega_{\text{D}})) + 3d_{\text{CH}}^2(\mathcal{J}_{\text{CH}}(\omega_C) + \mathcal{J}_{\text{CH}}(\omega_{\text{H}})) \\
&+ \frac{1}{6}d_{\text{CD}}^2(11\mathcal{J}_{\text{CD}}(\omega_C - \omega_{\text{D}}) + 9\mathcal{J}_{\text{CD}}(\omega_{\text{D}}) + 60\mathcal{J}_{\text{CD}}(\omega_C) + 66\mathcal{J}_{\text{CD}}(\omega_C + \omega_{\text{D}})) \\
&+ \frac{1}{6}d_{\text{HD}}^2(11\mathcal{J}_{\text{HD}}(\omega_{\text{H}} - \omega_{\text{D}}) + 9\mathcal{J}_{\text{HD}}(\omega_{\text{D}}) + 60\mathcal{J}_{\text{HD}}(\omega_{\text{H}}) + 66\mathcal{J}_{\text{HD}}(\omega_{\text{H}} + \omega_{\text{D}})) \\
&+ \frac{4}{3}d_{\text{DDvic}}^2(\mathcal{J}_{\text{DDvic}}(0) + 3\mathcal{J}_{\text{DDvic}}(\omega_{\text{D}}) + 6\mathcal{J}_{\text{DDvic}}(2\omega_{\text{D}})) \\
&+ \frac{4}{3}d_{\text{CDvic}}^2(3\mathcal{J}_{\text{CDvic}}(\omega_C) + \mathcal{J}_{\text{CDvic}}(\omega_C - \omega_{\text{D}}) + 6\mathcal{J}_{\text{CDvic}}(\omega_C + \omega_{\text{D}})) \\
&+ \frac{4}{3}d_{\text{HDvic}}^2(3\mathcal{J}_{\text{HDvic}}(\omega_{\text{H}}) + \mathcal{J}_{\text{HDvic}}(\omega_{\text{H}} - \omega_{\text{D}}) + 6\mathcal{J}_{\text{HDvic}}(\omega_{\text{H}} + \omega_{\text{D}})),
\end{aligned}$$

$$\begin{aligned}
R_{\text{CD}} &= \frac{3}{8}\zeta_{\mathcal{Q}}^2(\mathcal{J}_{\mathcal{Q}}(\omega_{\text{D}}) + 4\mathcal{J}_{\mathcal{Q}}(2\omega_{\text{D}})) + \frac{2}{3}\Delta\sigma_{\text{C}}^2\omega_{\text{C}}^2\mathcal{J}_{\text{C}}(\omega_{\text{C}}) \\
&+ \frac{1}{2}d_{\text{CH}}^2(\mathcal{J}_{\text{CH}}(\omega_{\text{C}} - \omega_{\text{H}}) + 3\mathcal{J}_{\text{CH}}(\omega_{\text{C}}) + 6\mathcal{J}_{\text{CH}}(\omega_{\text{C}} + \omega_{\text{H}})) \\
&+ \frac{1}{2}d_{\text{HD}}^2(\mathcal{J}_{\text{HD}}(\omega_{\text{H}} - \omega_{\text{D}}) + 3\mathcal{J}_{\text{HD}}(\omega_{\text{D}}) + 6\mathcal{J}_{\text{HD}}(\omega_{\text{H}} + \omega_{\text{D}})) \\
&+ \frac{4}{3}d_{\text{DD}}^2(\mathcal{J}_{\text{DD}}(0) + 3\mathcal{J}_{\text{DD}}(\omega_{\text{D}}) + 6\mathcal{J}_{\text{DD}}(2\omega_{\text{D}})) \\
&+ \frac{1}{6}d_{\text{CD}}^2(11\mathcal{J}_{\text{CD}}(\omega_{\text{C}} - \omega_{\text{D}}) + 9\mathcal{J}_{\text{CD}}(\omega_{\text{D}}) + 60\mathcal{J}_{\text{CD}}(\omega_{\text{C}}) + 66\mathcal{J}_{\text{CD}}(\omega_{\text{C}} + \omega_{\text{D}})) \\
&+ \frac{4}{3}d_{\text{DDvic}}^2(\mathcal{J}_{\text{DDvic}}(0) + 3\mathcal{J}_{\text{DDvic}}(\omega_{\text{D}}) + 6\mathcal{J}_{\text{DDvic}}(2\omega_{\text{D}})) \\
&+ \frac{4}{3}d_{\text{CDvic}}(\mathcal{J}_{\text{CDvic}}(\omega_{\text{C}} - \omega_{\text{D}}) + 3\mathcal{J}_{\text{CDvic}}(\omega_{\text{C}}) + 6\mathcal{J}_{\text{CDvic}}(\omega_{\text{C}} + \omega_{\text{D}})), \\
R_{\text{D}} &= \frac{3}{8}\zeta_{\mathcal{Q}}^2(\mathcal{J}_{\mathcal{Q}}(\omega_{\text{D}}) + 4\mathcal{J}_{\mathcal{Q}}(2\omega_{\text{D}})) + \frac{4}{3}d_{\text{DD}}^2(\mathcal{J}_{\text{DD}}(0) + 3\mathcal{J}_{\text{DD}}(\omega_{\text{D}}) + 6\mathcal{J}_{\text{DD}}(2\omega_{\text{D}})) \\
&+ \frac{1}{2}d_{\text{CD}}^2(\mathcal{J}_{\text{CD}}(\omega_{\text{C}} - \omega_{\text{D}}) + 3\mathcal{J}_{\text{CD}}(\omega_{\text{D}}) + 6\mathcal{J}_{\text{CD}}(\omega_{\text{C}} + \omega_{\text{D}})) \\
&+ \frac{1}{2}d_{\text{HD}}^2(\mathcal{J}_{\text{HD}}(\omega_{\text{H}} - \omega_{\text{D}}) + 3\mathcal{J}_{\text{HD}}(\omega_{\text{D}}) + 6\mathcal{J}_{\text{HD}}(\omega_{\text{H}} + \omega_{\text{D}})) \\
&+ \frac{4}{3}d_{\text{DDvic}}^2(\mathcal{J}_{\text{DDvic}}(0) + 3\mathcal{J}_{\text{DDvic}}(\omega_{\text{D}}) + 6\mathcal{J}_{\text{DDvic}}(2\omega_{\text{D}})), \\
R_{\text{CDD}}^{(1)} &= \frac{1}{24}\zeta_{\mathcal{Q}}^2(3\mathcal{J}_{\mathcal{Q}}(0) + 5\mathcal{J}_{\mathcal{Q}}(\omega_{\text{D}}) + 2\mathcal{J}_{\mathcal{Q}}(2\omega_{\text{D}})) + \frac{3}{2}d_{\text{DD}}\zeta_{\mathcal{Q}}(2\mathcal{J}_{\text{DD},\mathcal{Q}}(0) + 3\mathcal{J}_{\text{DD},\mathcal{Q}}(\omega_{\text{D}})) \\
&+ \frac{2}{3}\Delta\sigma_{\text{C}}^2\omega_{\text{C}}^2\mathcal{J}_{\text{C}}(\omega_{\text{C}}) + \frac{1}{2}d_{\text{CH}}^2(\mathcal{J}_{\text{CH}}(\omega_{\text{C}} - \omega_{\text{H}}) + 3\mathcal{J}_{\text{CH}}(\omega_{\text{C}}) + 6\mathcal{J}_{\text{CH}}(\omega_{\text{C}} + \omega_{\text{H}})) \\
&+ \frac{1}{2}d_{\text{DD}}^2(7\mathcal{J}_{\text{DD}}(0) + 18\mathcal{J}_{\text{DD}}(\omega_{\text{D}}) + 12\mathcal{J}_{\text{DD}}(2\omega_{\text{D}})) \\
&+ \frac{1}{2}d_{\text{HD}}^2(4\mathcal{J}_{\text{HD}}(0) + \mathcal{J}_{\text{HD}}(\omega_{\text{H}} - \omega_{\text{D}}) + 3\mathcal{J}_{\text{HD}}(\omega_{\text{D}}) + 6\mathcal{J}_{\text{HD}}(\omega_{\text{H}}) + 6\mathcal{J}_{\text{HD}}(\omega_{\text{H}} + \omega_{\text{D}})) \\
&+ \frac{1}{2}d_{\text{CD}}^2(4\mathcal{J}_{\text{CD}}(0) + 5\mathcal{J}_{\text{CD}}(\omega_{\text{C}} - \omega_{\text{D}}) + 3\mathcal{J}_{\text{CD}}(\omega_{\text{D}}) + 6\mathcal{J}_{\text{CD}}(\omega_{\text{C}}) + 30\mathcal{J}_{\text{CD}}(\omega_{\text{C}} + \omega_{\text{D}})) \\
&+ \frac{4}{3}d_{\text{CDvic}}(\mathcal{J}_{\text{CDvic}}(\omega_{\text{C}} - \omega_{\text{D}}) + 3\mathcal{J}_{\text{CDvic}}(\omega_{\text{C}}) + 6\mathcal{J}_{\text{CDvic}}(\omega_{\text{C}} + \omega_{\text{D}})) - 2d_{\text{CD}}^2\mathcal{J}_{\text{CD}_1,\text{CD}_2}(0) \\
&+ \frac{4}{3}d_{\text{DDvic}}^2(5\mathcal{J}_{\text{DDvic}}(0) + 9\mathcal{J}_{\text{DDvic}}(\omega_{\text{D}}) + 6\mathcal{J}_{\text{DDvic}}(2\omega_{\text{D}})) \\
&- d_{\text{HD}}^2(2\mathcal{J}_{\text{HD}_1,\text{HD}_2}(0) + 3\mathcal{J}_{\text{HD}_1,\text{HD}_2}(\omega_{\text{H}})) - \frac{8}{3}d_{\text{DD}}^2(2\mathcal{J}_{\text{D}_1\text{Dvic},\text{D}_2\text{Dvic}}(0) + 3\mathcal{J}_{\text{D}_1\text{Dvic},\text{D}_2\text{Dvic}}(\omega_{\text{D}})),
\end{aligned}$$

$$\begin{aligned}
R_{CDD}^{(2)} &= \frac{3}{4}\zeta_{\mathcal{Q}}(\mathcal{J}_{\mathcal{Q}}(\omega_{\text{D}}) + 4\mathcal{J}_{\mathcal{Q}}(2\omega_{\text{D}})) + \frac{2}{3}\Delta\sigma_{\text{C}}^2\omega_{\text{C}}^2\mathcal{J}_{\text{C}}(\omega_{\text{C}}) \\
&+ \frac{1}{2}d_{\text{CH}}^2(\mathcal{J}_{\text{CH}}(\omega_{\text{C}} - \omega_{\text{H}}) + 3\mathcal{J}_{\text{CH}}(\omega_{\text{C}}) + 6\mathcal{J}_{\text{CH}}(\omega_{\text{C}} + \omega_{\text{H}})) \\
&+ d_{\text{CD}}^2(\mathcal{J}_{\text{CD}}(\omega_{\text{C}} - \omega_{\text{D}}) + 3\mathcal{J}_{\text{CD}}(\omega_{\text{D}}) + 6\mathcal{J}_{\text{CD}}(\omega_{\text{C}} + \omega_{\text{D}}) + 12\mathcal{J}_{\text{CD}}(\omega_{\text{C}})) \\
&+ d_{\text{HD}}^2(\mathcal{J}_{\text{HD}}(\omega_{\text{H}} - \omega_{\text{D}}) + 3\mathcal{J}_{\text{HD}}(\omega_{\text{D}}) + 6\mathcal{J}_{\text{HD}}(\omega_{\text{H}} + \omega_{\text{D}})) \\
&+ d_{\text{DD}}^2(\mathcal{J}_{\text{DD}}(0) + 12\mathcal{J}_{\text{DD}}(\omega_{\text{D}}) + 6\mathcal{J}_{\text{DD}}(2\omega_{\text{D}})) \\
&+ \frac{4}{3}d_{\text{CDvic}}^2(\mathcal{J}_{\text{CDvic}}(\omega_{\text{C}} - \omega_{\text{D}}) + 3\mathcal{J}_{\text{CDvic}}(\omega_{\text{C}}) + 6\mathcal{J}_{\text{CDvic}}(\omega_{\text{C}} + \omega_{\text{D}})) \\
&+ \frac{8}{3}d_{\text{DDvic}}(\mathcal{J}_{\text{DDvic}}(0) + 3\mathcal{J}_{\text{DDvic}}(\omega_{\text{D}}) + 6\mathcal{J}_{\text{DDvic}}(2\omega_{\text{D}})), \\
R &= \frac{9}{8}\zeta_{\mathcal{Q}}^2\mathcal{J}_{\mathcal{Q}}(\omega_{\text{D}}) + \frac{2}{3}\Delta\sigma_{\text{C}}^2\omega_{\text{C}}^2\mathcal{J}_{\text{C}}(\omega_{\text{C}}) \\
&+ \frac{1}{2}d_{\text{CH}}^2(\mathcal{J}_{\text{CH}}(\omega_{\text{C}} - \omega_{\text{H}}) + 3\mathcal{J}_{\text{CH}}(\omega_{\text{C}}) + 6\mathcal{J}_{\text{CH}}(\omega_{\text{C}} + \omega_{\text{H}})) \\
&+ \frac{3}{2}d_{\text{CD}}^2(\mathcal{J}_{\text{CD}}(\omega_{\text{C}} - \omega_{\text{D}}) + 3\mathcal{J}_{\text{CD}}(\omega_{\text{D}}) + 4\mathcal{J}_{\text{CD}}(\omega_{\text{C}}) + 6\mathcal{J}_{\text{CD}}(\omega_{\text{C}} + \omega_{\text{D}})) \\
&+ \frac{3}{2}d_{\text{HD}}^2(\mathcal{J}_{\text{HD}}(\omega_{\text{H}} - \omega_{\text{D}}) + 3\mathcal{J}_{\text{HD}}(\omega_{\text{D}}) + 6\mathcal{J}_{\text{HD}}(\omega_{\text{H}} + \omega_{\text{D}})) \\
&+ 4d_{\text{DD}}^2(\mathcal{J}_{\text{DD}}(0) + 3\mathcal{J}_{\text{DD}}(\omega_{\text{D}}) + 6\mathcal{J}_{\text{DD}}(2\omega_{\text{D}})) \\
&+ \frac{4}{3}d_{\text{CDvic}}^2(\mathcal{J}_{\text{CDvic}}(\omega_{\text{C}} - \omega_{\text{D}}) + 3\mathcal{J}_{\text{CDvic}}(\omega_{\text{C}}) + 6\mathcal{J}_{\text{CDvic}}(\omega_{\text{C}} + \omega_{\text{D}})) \\
&+ 4d_{\text{DDvic}}^2(\mathcal{J}_{\text{DDvic}}(0) + 3\mathcal{J}_{\text{DDvic}}(\omega_{\text{D}}) + 6\mathcal{J}_{\text{DDvic}}(2\omega_{\text{D}})).
\end{aligned}$$

1102 4.3. Cross-relaxation rates

1103 Cross-relaxation rates with the operator \hat{C}_z are:

$$\begin{aligned}
\sigma_{\text{CH}} &= \frac{1}{2}d_{\text{CH}}^2(-\mathcal{J}_{\text{CH}}(\omega_{\text{C}} - \omega_{\text{H}}) + 6\mathcal{J}_{\text{CH}}(\omega_{\text{C}} + \omega_{\text{H}})), \\
\eta_z^{\text{C}} &= -2\Delta\sigma_{\text{C}}\omega_{\text{C}}d_{\text{CH}}\mathcal{J}_{\text{C,CH}}(\omega_{\text{C}}), \\
\kappa^{\text{C}} &= 2\sqrt{6}d_{\text{CH}}d_{\text{CD}}\mathcal{J}_{\text{CH,CD}}(\omega_{\text{C}}), \\
\eta_z^{\text{CD}} &= -4\sqrt{\frac{2}{3}}d_{\text{CD}}\Delta\sigma_{\text{C}}\omega_{\text{C}}\mathcal{J}_{\text{C,CD}}(\omega_{\text{C}}), \\
\sigma_{\text{CD}} &= \sqrt{\frac{2}{3}}d_{\text{CD}}^2(-\mathcal{J}_{\text{CD}}(\omega_{\text{C}} - \omega_{\text{D}}) + 6\mathcal{J}_{\text{CD}}(\omega_{\text{C}} + \omega_{\text{D}})), \\
\lambda &= \frac{4}{3}d_{\text{CD}}^2(\mathcal{J}_{\text{CD,CD}}(\omega_{\text{C}} - \omega_{\text{D}}) + 6\mathcal{J}_{\text{CD,CD}}(\omega_{\text{C}} + \omega_{\text{D}})), \\
\nu_z &= 8d_{\text{CD}}^2\mathcal{J}_{\text{CD,CD}}(\omega_{\text{C}}), \\
\mu &= \frac{\sqrt{2}}{3}d_{\text{CD}}^2(-\mathcal{J}_{\text{CD}}(\omega_{\text{C}} - \omega_{\text{D}}) + 6\mathcal{J}_{\text{CD}}(\omega_{\text{C}}) - 6\mathcal{J}_{\text{CD}}(\omega_{\text{C}} + \omega_{\text{D}})).
\end{aligned}$$

Finally, other cross-relaxation rates are:

$$\begin{aligned}
\kappa^{\text{H}} &= 2\sqrt{6}d_{\text{CH}}d_{\text{HD}}\mathcal{J}_{\text{CH,HD}}(\omega_{\text{H}}), \\
\kappa^{\text{CH}} &= -4\sqrt{\frac{2}{3}}d_{\text{CD}}\Delta\sigma_{\text{C}}\omega_{\text{C}}\mathcal{J}_{\text{CD,CC}}(\omega_{\text{C}}), \\
\kappa^{\text{CD}} &= 8d_{\text{CD}}^2\mathcal{J}_{\text{CD}_1,\text{CD}_2}(\omega_{\text{C}}) - \frac{4}{3}d_{\text{DD}}^2(\mathcal{J}_{\text{DD}}(0) - 6\mathcal{J}_{\text{DD}}(2\omega_{\text{D}})), \\
\kappa^{\text{CHD}} &= 8d_{\text{CD}}^2\mathcal{J}_{\text{CD}_1,\text{CD}_2}(\omega_{\text{C}}) + 8d_{\text{HD}}^2\mathcal{J}_{\text{HD}_1,\text{HD}_2}(\omega_{\text{H}}) - \frac{4}{3}d_{\text{DD}}^2(\mathcal{J}_{\text{DD}}(0) - 6\mathcal{J}_{\text{DD}}(2\omega_{\text{D}})), \\
\kappa^{\text{CDD}} &= -\frac{3}{2}d_{\text{DD}}^2\mathcal{J}_{\text{DD}}(0), \\
\sigma_{\text{HD}} &= \sqrt{\frac{2}{3}}d_{\text{HD}}^2(-\mathcal{J}_{\text{HD}}(\omega_{\text{H}} - \omega_{\text{D}}) + 6\mathcal{J}_{\text{HD}}(\omega_{\text{H}} + \omega_{\text{D}})), \\
\sigma_{\text{DD}} &= \frac{4}{3}d_{\text{DD}}^2(-\mathcal{J}_{\text{DD}}(0) + 6\mathcal{J}_{\text{DD}}(2\omega_{\text{D}})), \\
\sigma_{\text{CHD}} &= 3d_{\text{CD}}d_{\text{HD}}\mathcal{J}_{\text{CD,HD}}(\omega_{\text{D}}), \\
\eta_z^{\text{CHD}} &= -2d_{\text{CH}}\Delta\sigma_{\text{C}}\omega_{\text{C}}\mathcal{J}_{\text{C,CH}}(\omega_{\text{C}}), \\
\delta &= \frac{12}{\sqrt{6}}d_{\text{CH}}d_{\text{CD}}\mathcal{J}_{\text{CH,CD}}(\omega_{\text{C}}) - \frac{2}{\sqrt{6}}d_{\text{HD}}^2(\mathcal{J}_{\text{HD}}(\omega_{\text{H}} - \omega_{\text{D}}) - 6\mathcal{J}_{\text{HD}}(\omega_{\text{H}} + \omega_{\text{D}})),
\end{aligned}$$

$$\begin{aligned}
\lambda^{(1)} &= \sqrt{\frac{1}{6}} d_{\text{HD}}^2 (\mathcal{J}_{\text{HD}_1, \text{HD}_2}(\omega_{\text{H}} - \omega_{\text{D}}) - 6\mathcal{J}_{\text{HD}_1, \text{HD}_2}(\omega_{\text{H}} + \omega_{\text{D}})) \\
&\quad + \frac{2}{\sqrt{6}} d_{\text{HD}} d_{\text{DD}} (2\mathcal{J}_{\text{HD}, \text{DD}}(0) - 3\mathcal{J}_{\text{HD}, \text{DD}}(\omega_{\text{D}})), \\
\lambda^{(2)} &= -\frac{2}{\sqrt{6}} d_{\text{CD}} d_{\text{DD}} (2\mathcal{J}_{\text{CD}, \text{DD}}(0) + 3\mathcal{J}_{\text{CD}, \text{DD}}(\omega_{\text{D}})), \\
\nu_z^{(1)} &= -\sqrt{\frac{2}{3}} d_{\text{HD}}^2 (\mathcal{J}_{\text{HD}}(\omega_{\text{H}} - \omega_{\text{D}}) - 6\mathcal{J}_{\text{HD}}(\omega_{\text{H}} + \omega_{\text{D}})) \\
&\quad + \sqrt{3} (d_{\text{CH}} d_{\text{CD}} \mathcal{J}_{\text{CH}, \text{CD}}(\omega_{\text{C}}) + d_{\text{HD}} d_{\text{DD}} \mathcal{J}_{\text{HD}, \text{DD}}(\omega_{\text{D}})), \\
\nu_z^{(2)} &= -4\sqrt{\frac{2}{3}} d_{\text{CD}} \Delta\sigma_C \omega_C \mathcal{J}_{\text{C}, \text{CD}}(\omega_C), \\
\nu_z^{(3)} &= 2\sqrt{6} d_{\text{CD}} d_{\text{DD}} \mathcal{J}_{\text{CD}, \text{DD}}(\omega_{\text{D}}), \\
\nu_z^{(4)} &= d_{\text{DD}}^2 (\mathcal{J}_{\text{DD}}(0) - 3\mathcal{J}_{\text{DD}}(\omega_{\text{D}})) - \frac{3}{4} d_{\text{DD}} \zeta_{\mathcal{Q}} (\mathcal{J}_{\text{DD}, \mathcal{Q}}(0) - 3\mathcal{J}_{\text{DD}, \mathcal{Q}}(\omega_{\text{D}}) + 6\mathcal{J}_{\text{DD}, \mathcal{Q}}(2\omega_{\text{D}})) \\
&\quad - \frac{3}{2} d_{\text{CD}}^2 \mathcal{J}_{\text{CD}, \text{CD}}(\omega_{\text{D}}) - \frac{1}{2} d_{\text{HD}}^2 (\mathcal{J}_{\text{HD}, \text{HD}}(\omega_{\text{H}} - \omega_{\text{D}}) + 3\mathcal{J}_{\text{HD}, \text{HD}}(\omega_{\text{D}}) + 6\mathcal{J}_{\text{HD}, \text{HD}}(\omega_{\text{H}} + \omega_{\text{D}})) \\
&\quad - \frac{4}{3} d_{\text{DD}, \text{vic}}^2 (\mathcal{J}_{\text{D}_1 \text{D}_{\text{vic}}, \text{D}_2 \text{D}_{\text{vic}}}(0) + 3\mathcal{J}_{\text{D}_1 \text{D}_{\text{vic}}, \text{D}_2 \text{D}_{\text{vic}}}(\omega_{\text{D}}) + 6\mathcal{J}_{\text{D}_1 \text{D}_{\text{vic}}, \text{D}_2 \text{D}_{\text{vic}}}(2\omega_{\text{D}})), \\
\mu^{(1)} &= -\frac{\sqrt{3}}{2} d_{\text{HD}}^2 (\mathcal{J}_{\text{HD}}(\omega_{\text{H}} - \omega_{\text{D}}) - 6\mathcal{J}_{\text{HD}}(\omega_{\text{H}} + \omega_{\text{D}})) + 2\sqrt{3} d_{\text{CH}} d_{\text{CD}} \mathcal{J}_{\text{CH}, \text{CD}}(\omega_C) \\
&\quad - \frac{3\sqrt{3}}{2} d_{\text{HD}} \zeta_{\mathcal{Q}} \mathcal{J}_{\mathcal{Q}, \text{HD}}(\omega_{\text{D}}), \\
\mu^{(2)} &= -\frac{4}{\sqrt{3}} d_{\text{CD}} \Delta\sigma_C \omega_C \mathcal{J}_{\text{C}, \text{CD}}(\omega_C), \\
\mu^{(3)} &= \frac{\sqrt{3}}{6} d_{\text{CD}}^2 (\mathcal{J}_{\text{CD}}(\omega_C - \omega_{\text{D}}) - 6\mathcal{J}_{\text{CD}}(\omega_C + \omega_{\text{D}})) - \frac{3\sqrt{3}}{2} d_{\text{CD}} \zeta_{\mathcal{Q}} \mathcal{J}_{\mathcal{Q}, \text{CD}}(\omega_{\text{D}}), \\
\mu^{(4)} &= -\frac{\sqrt{2}}{2} d_{\text{DD}}^2 (2\mathcal{J}_{\text{DD}}(0) + 3\mathcal{J}_{\text{DD}}(\omega_{\text{D}})) - \frac{\sqrt{2}}{3} d_{\text{CD}}^2 (\mathcal{J}_{\text{CD}, \text{CD}}(\omega_C - \omega_{\text{D}}) + 6\mathcal{J}_{\text{CD}, \text{CD}}(\omega_C + \omega_{\text{D}})) \\
&\quad + \frac{3}{4\sqrt{2}} d_{\text{DD}} \zeta_{\mathcal{Q}} (\mathcal{J}_{\mathcal{Q}, \text{DD}}(0) + \mathcal{J}_{\mathcal{Q}, \text{DD}}(\omega_{\text{D}}) - 2\mathcal{J}_{\mathcal{Q}, \text{DD}}(2\omega_{\text{D}})), \\
\mu^{(5)} &= -\sqrt{2} d_{\text{DD}}^2 (\mathcal{J}_{\text{DD}}(0) - 6\mathcal{J}_{\text{DD}}(2\omega_{\text{D}})) + 4\sqrt{2} d_{\text{CD}}^2 \mathcal{J}_{\text{CD}_1, \text{CD}_1}(\omega_C) - 3\sqrt{2} d_{\text{DD}} \zeta_{\mathcal{Q}} \mathcal{J}_{\mathcal{Q}, \text{DD}}(\omega_{\text{D}}).
\end{aligned}$$

1104 5. Figures

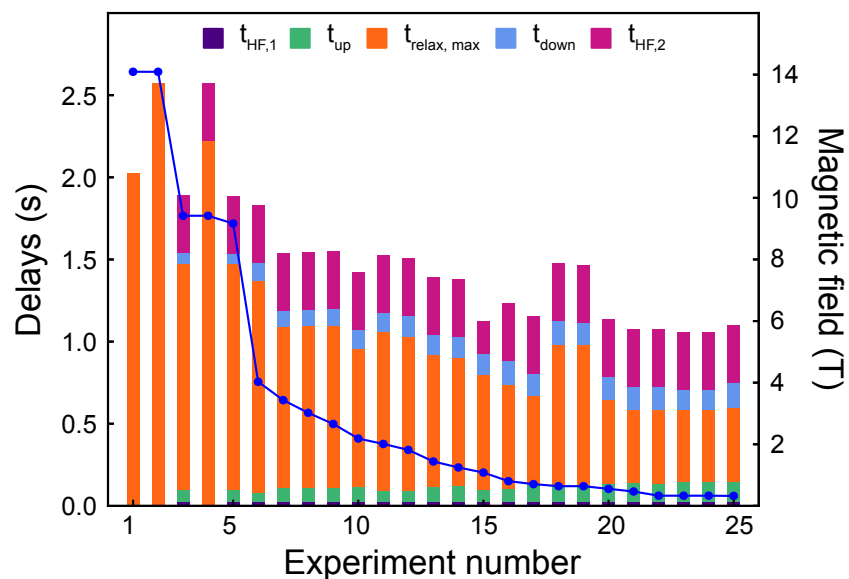


Figure S2: Experimental delays for the 25 experiments used in the analysis of the dynamics of isoleucine- δ 1-methyl groups of Ubiquitin, and ordered from the highest magnetic field at which relaxation takes place to the lowest. The time labels refer to the decomposition of the free-relaxation part of the pulse-sequence, as shown in Fig. 3 of the main text. The blue curve (right y-axis) shows the variation of the magnetic field for each experiment (associated with an increase of shuttling height). Experiments 1, 2 and 4 were performed on high-field spectrometers, with no shuttle.

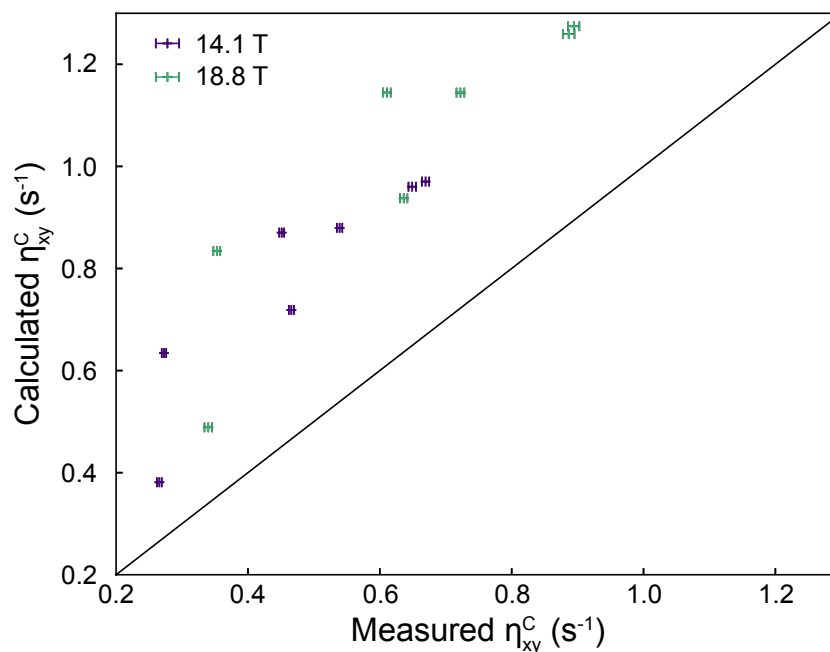


Figure S3: Correlation plot between the calculated and measured transverse CSA/DD cross-correlated cross-relaxation rates at 14.1 T and 18.8 T, with no scaling of the CSA.

1105 **6. Hamiltonian in REDKITE**

1106 We report here the definition of the Hamiltonian as written in REDKITE.

1107 Constants are defined in Table S2.

1108 For the dipolar interaction:

1109
$$\text{HDD}[i_ , j_ , t_] := \sqrt{6} \text{dDD}[\text{Nuclei}[[i, 2]], \text{Nuclei}[[j, 2]]] \times \text{Sum} [(-1)^m$$

 1110
$$\text{M}[m, \text{opTDipFreq}[\{\text{Nuclei}[[i, 1]], \text{Nuclei}[[j, 1]]\}, \{-m, k\}], t, \Phi[\text{Nuclei}[[i, 2]],$$

 1111
$$\text{Nuclei}[[j, 2]]] \text{opTDip}[\{\text{Nuclei}[[i, 1]], \text{Nuclei}[[j, 1]]\}, \{-m, k\}], \{m, -2, 2\}], \{k,$$

 1112
$$\text{Min}[0, \text{Abs}[m]-1], \text{Min}[1, 2 - \text{Abs}[m]]];$$

 1113
$$\text{HDDtot}[t_] := \text{Sum}[\text{HDD}[i, j, t], \{i, 1, \text{NumberOfAtoms}-1\}, \{j,$$

 1114
$$i+1, \text{NumberOfAtoms}\}];$$

1115 For the CSA interaction, in the case of an axially symmetric tensor:

1116
$$\text{HCSA}[t_] := \text{Sum}[\text{CSAConsidered}[[n]] \text{Sum} [(-1)^m \Delta_{\text{Nuclei}[[n, 2]]} \text{M}[m,$$

 1117
$$\text{opTCSAFreq}[\text{Nuclei}[[n, 1]], \{-m, 0\}], t, \text{AngleCSA}[[n, 1]]]$$

 1118
$$\text{opTCSA}[\text{Nuclei}[[n, 1]], \{-m, 0\}], \{m, -2, 2\}], \{n, 1, \text{NumberOfAtoms}\}];$$

1119 and for an asymmetric tensor:

$$\begin{aligned} 1120 \quad \text{HCSA}[t_] &:= \text{Sum}[\text{CSAConsidered}[[n]] \text{Sum} [(-1)^m \left(\sigma \ln_{\text{Nuclei}[[n,2]]} M[m, \right. \\ 1121 \quad \text{opTCSAFreq}[\text{Nuclei}[[n,1]],\{-m,0\}], t, \text{AngleCSA}[[n, 1]]] &+ \sigma \rho n_{\text{Nuclei}[[n,2]]} M[m, \\ 1122 \quad \quad \quad \text{opTCSAFreq}[\text{Nuclei}[[n,1]],\{-m,0\}], t, \text{AngleCSA}[[n, 2]]] &\left. \right) \\ 1123 \quad \quad \quad \text{opTCSA}[\text{Nuclei}[[n,1]],\{-m,0\}], \{m, -2, 2\}, \{n, 1, \text{NumberOfAtoms}\}]; \end{aligned}$$

1124 and for the quadrupolar interaction:

$$\begin{aligned} 1125 \quad \text{HQuad}[i_ , t_] &:= \frac{d_Q[\text{AtomsQuadConsidered}[[i,2]]]}{4\text{QuantumNumberConsidered}[[i]](2\text{QuantumNumberConsidered}[[i]]-1)} \\ 1126 \quad \text{Sum} [(-1)^k M[m, \text{opTQuadFreq}[\text{Atoms}[[i, 1]], \{-m, 0\}], t, \text{AngleQ}[[i]]] &V_k \\ 1127 \quad \text{opTQuad}[\text{AtomsQuadConsidered}[[n,2]],\{-m,0\}], \{m, -2, 2\}, \{k, -2, 2\}]; \end{aligned}$$

Table S2: Variable names used in REDKITE.

Name	definition	User-defined?
Atoms	Table containing the spins present in the system and their associated labels	Yes
NumberOfAtoms	number of spins considered	No
LF	vector orienting the System Frame in the Cartesian axis system	Yes
Coordinates	Table containing the position of the spins in the Cartesian axis system	Yes
CSAConsidered	Table filled with 1 (CSA is considered) or 0 (CSA is neglected)	Yes
$\delta_{csa}[i]$	value of the axially symmetric CSA associated with nucleus i	Yes
$\sigma_{long}[i]$	value of the longitudinal component of an asymmetric CSA associated with nucleus i	Yes
$\sigma_{perp}[i]$	value of the orthogonal component of an asymmetric CSA associated with nucleus i	Yes
vectorNum ^{"CSA"} _{i}	orientation of the principal axis of a symmetric CSA tensor for spin i	Yes
vectorNuml ^{"CSA"} _{i}	orientation of the longitudinal component of a symmetric CSA tensor for spin i	Yes
vectorNump ^{"CSA"} _{i}	orientation of the longitudinal component of a symmetric CSA tensor for spin i	Yes
$d_Q[i]$	strength of the quadrupolar interaction for spin i	Yes
vectorNum ^{"Quad"} _{i}	orientation of the quadrupolar interaction for spin i	Yes
opTDip	tensors associated with dipolar interactions	No
opTCSA	tensors associated with CSA interactions	No
opTQuad	tensors associated with quadrupolar interactions	No
opTDipFreq	frequencies associated to tensors OpTDip	No
opTCSAFreq	frequencies associated to tensors OpTCSA	No
opTQuadFreq	frequencies associated to tensors OpTQuad	No
dDD[i, j]	dipolar coefficient for the interaction of spins i and j	No
$\Phi[i, j]$	vector linking spins i and j	No
Δ_i	symmetric CSA value in Hz: $\sqrt{2/3}\delta_{csa}[i]\omega[i]$	No

Continued on next page

Table S2 – continued from previous page

Name	definition	User-defined?
σ_{ln_i}	longitudinal component of an asymmetric CSA value in Hz: $\sqrt{2/3}\sigma_{\text{long}[i]}\omega[i]$	No
σ_{pn_i}	orthogonal component of an asymmetric CSA value in Hz: $\sqrt{2/3}\sigma_{\text{perp}[i]}\omega[i]$	No
$\omega[i]$	Larmor frequency associated with spin i	No
AngleCSA[n, 1]	orientation of the longitudinal component of the CSA of spin i	No
AngleCSA[n, 2]	orientation of the orthogonal component of the CSA of spin i	No
AngleQ[n, 2]	orientation of the quadrupolar interaction of spin i	No
M	function depending on variables detailed in main text to perform the calculations	No
SpinTermOfInterest	Studied operator during the relaxation experiments	Yes

Table S3: Tensor operators for the dipole-dipole interaction and associated frequency as written in REDKITE. Tensors are of rank 2 and with coherence order q . The letter p refers to the decomposition of the tensors in the irreducible tensor operator basis. Tensors are written $\text{opTDip}[\{i_-, j_-\}, \{q, p\}]$ for the interaction between nuclei i and j . The associated frequencies are $\text{opTDipFreq}[\{i_-, j_-\}, \{q, p\}]$. We define $\omega[i] = -\gamma_i B_0$ in REDKITE. B_0 is the magnetic field.

coherence order	p	Tensor	Frequency
2	0	$\frac{1}{2}\text{opI}[i, " + "] \cdot \text{opI}[j, " + "]$	$\omega[i] + \omega[j]$
1	0	$-\frac{1}{2}\text{opI}[i, " z "] \cdot \text{opI}[j, " + "]$	$\omega[j]$
1	1	$-\frac{1}{2}\text{opI}[i, " + "] \cdot \text{opI}[j, " z "]$	$\omega[i]$
0	-1	$-\frac{1}{2\sqrt{6}}\text{opI}[i, " - "] \cdot \text{opI}[j, " + "]$	$\omega[j] - \omega[i]$
0	0	$\frac{2}{\sqrt{6}}\text{opI}[i, " z "] \cdot \text{opI}[j, " z "]$	0
0	1	$-\frac{1}{2\sqrt{6}}\text{opI}[i, " + "] \cdot \text{opI}[j, " - "]$	$\omega[i] - \omega[j]$
-1	0	$\frac{1}{2}\text{opI}[i, " z "] \cdot \text{opI}[j, " - "]$	$\omega[j]$
-1	1	$\frac{1}{2}\text{opI}[i, " - "] \cdot \text{opI}[j, " z "]$	$\omega[i]$
-2	0	$\frac{1}{2}\text{opI}[i, " - "] \cdot \text{opI}[j, " - "]$	$-\omega[i] - \omega[j]$

Table S4: Tensor operators for the Chemical Shift Anisotropy (CSA) interaction and associated frequency as written in REDKITE. Tensors are of rank 2 and with coherence order q . The letter p refers to the decomposition of the tensors in the irreducible tensor operator basis. Tensors are written $\text{opTDip}[\{i_-, j_-\}, \{q, p\}]$ for the interaction between nuclei i and j . The associated frequencies are $\text{opTDipFreq}[\{i_-, j_-\}, \{q, p\}]$. We define $\omega[i] = -\gamma_i B_0$ in REDKITE. B_0 is the magnetic field.

coherence order	p	Tensor	Frequency
2	0	0	$2\omega[i]$
1	0	$-\frac{1}{2}\text{opI}[i, " + "]$	$\omega[i]$
0	0	$\frac{2}{\sqrt{6}}\text{opI}[i, " z "]$	0
-1	0	$\frac{1}{2}\text{opI}[i, " - "]$	$-\omega[i]$
-2	0	0	$-2\omega[i]$

Table S5: Tensor operators for the quadrupolar interaction and associated frequency as written in REDKITE. Tensors are of rank 2 and with coherence order q . The letter p refers to the decomposition of the tensors in the irreducible tensor operator basis. Tensors are written `opTDip` $\{i_-, j_-\}$, $\{q, p\}$ for the interaction between nuclei i and j . The associated frequencies are `opTDipFreq` $\{i_-, j_-\}$, $\{q, p\}$. We define $\omega[i] = -\gamma_i B_0$ in REDKITE. B_0 is the magnetic field.

coherence order	p	Tensor	Frequency
2	0	$\frac{1}{2}\text{opI}[i, " + "] \cdot \text{opI}[i, " + "]$	$2\omega[i]$
1	0	$-\frac{1}{2}(\text{opI}[i, " z"] \cdot \text{opI}[i, " + "] + \text{opI}[i, " + "] \cdot \text{opI}[i, " z"])$	$\omega[i]$
0	0	$\frac{1}{\sqrt{6}}(2\text{opI}[i, " z"] \cdot \text{opI}[i, " z"] - \text{opI}[i, " x"] \cdot \text{opI}[i, " x"] - \text{opI}[i, " y"] \cdot \text{opI}[i, " y"])$	0
-1	0	$\frac{1}{2}(\text{opI}[i, " z"] \cdot \text{opI}[i, " - "] + \text{opI}[i, " - "] \cdot \text{opI}[i, " z"])$	$-\omega[i]$
-2	0	$\frac{1}{2}\text{opI}[i, " - "] \cdot \text{opI}[i, " - "]$	$-2\omega[i]$

Table S6: Values of the parameters describing the position of the effective surrounding deuterium nucleus for each isoleucine residue in the Cartesian axis system which origin is occupied by the ^{13}C .

Residue	3	13	23	30	36	44	61
$r_{y,\text{CD}_{\text{vic}}} (\text{\AA})$	-1.96	-1.97	-1.88	-2.00	-1.97	-1.17	-1.39
$r_{z,\text{CD}_{\text{vic}}} (\text{\AA})$	-0.73	-1.06	-0.86	-0.74	-0.65	-1.54	-1.44

Table S7: Longitudinal and transverse cross-correlated cross-relaxation rates between ^{13}C and ^{13}C , ^1H two spin order for the 7 isoleucine residues of Ubiquitin measured at 14.1 and 18.8 T.

residue	η_z^C/s^{-1} (14.1 T)	η_z^C/s^{-1} (18.8 T)	η_{xy}^C/s^{-1} (14.1 T)	η_{xy}^C/s^{-1} (18.8 T)
3	0.0413 ± 0.0006	0.0312 ± 0.0019	0.669 ± 0.006	0.894 ± 0.008
13	0.0524 ± 0.0005	0.0469 ± 0.0016	0.466 ± 0.004	0.636 ± 0.006
23	0.0208 ± 0.0007	0.0209 ± 0.0016	0.273 ± 0.003	0.353 ± 0.005
30	0.0505 ± 0.0007	0.0411 ± 0.0018	0.649 ± 0.006	0.886 ± 0.009
36	0.0585 ± 0.0007	0.0513 ± 0.0017	0.539 ± 0.004	0.722 ± 0.006
44	0.0492 ± 0.0003	0.0509 ± 0.0018	0.266 ± 0.004	0.340 ± 0.006
61	0.0376 ± 0.0006	0.0353 ± 0.0015	0.451 ± 0.004	0.611 ± 0.006

Table S8: Proton longitudinal relaxation rates of the 7 isoleucine residues of Ubiquitin measured at 14.1 and 18.8 T.

residue	$R_1(^1H)/s^{-1}$ (14.1 T)	$R_1(^1H)/s^{-1}$ (18.8 T)
3	0.235 ± 0.003	0.228 ± 0.001
13	0.344 ± 0.003	0.317 ± 0.001
23	0.572 ± 0.005	0.522 ± 0.002
30	0.258 ± 0.003	0.243 ± 0.001
36	0.305 ± 0.003	0.266 ± 0.001
44	0.292 ± 0.003	0.253 ± 0.001
61	0.430 ± 0.004	0.390 ± 0.001

Table S9: ^{13}C relaxation rate measured at 14.1 T following a relaxometry scheme (*i.e.* without control of the cross-relaxation pathways). The rate R_1^{app} was measured with the same delays as used in the standard relaxation experiment. The rate $R_1^{\prime\text{app}}$ was measured by adding an extra relaxation delay of 550 ms in all experiments.

residue	$R_1^{\text{app}}(^{13}C)/s^{-1}$	$R_1^{\prime\text{app}}(^{13}C)/s^{-1}$
3	0.349 ± 0.009	0.344 ± 0.011
13	0.455 ± 0.007	0.452 ± 0.010
23	0.603 ± 0.008	0.576 ± 0.011
30	0.385 ± 0.009	0.391 ± 0.011
36	0.445 ± 0.008	0.431 ± 0.010
44	0.429 ± 0.008	0.412 ± 0.010
61	0.497 ± 0.007	0.493 ± 0.010